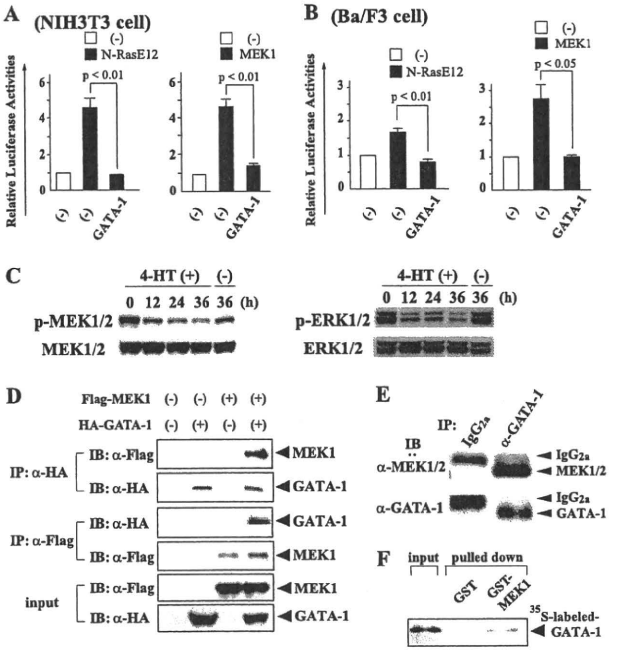

FIGURE 4. **GATA-1 blocks the Ras/Raf/MEK/ERK pathway through its direct interaction with MEK1.** *A*, NIH3T3 cells (2×10^5 cells seeded in 60-mm dish) were transfected with the indicated expression vectors and the reporter gene ($3 \times$ AP-1-Luc) together with pRL-CMV. After 12 h, the cells were serum-deprived for 24 h, then lysed, and subjected to the measurement of the firefly and *Renilla* luciferase activities. The relative firefly luciferase activities normalized by the *Renilla* luciferase activities are shown as means ± S.D. of three separate experiments. *B*, Ba/F3 cells (2×10^6 cells) were transfected with the same vectors as Fig. 4*A* using Amaxa Nucleofector technology. After 24 h of culture, the cells were lysed and subjected to the measurement of the luciferase activities. *C*, Ba/F3/N-RasE12/G1ERT cells cultured in RPMI supplemented with 1% FBS were treated with 1 μM 4-HT or vehicle. Total cellular lysates were prepared at the indicated time and subjected to immunoblotting with the indicated Abs. The filters were reprobed with corresponding Abs to confirm that the equal amounts of the proteins were loaded. *D*, coimmunoprecipitation analyses were performed using 293T cells transfected with HA-tagged GATA-1 and/or Flag-tagged MEK1 as indicated. *IP*, immunoprecipitation; *IB*, immunoblotting; α, anti. *E*, total cellular lysate was prepared from murine BM CD71$^+$ cells. Immunoprecipitation and immunoblot analyses were performed with the indicated antibodies. F. The *in vitro* binding between GATA-1 and MEK1 was examined by GST pull-down assays. ^{35}S-labeled GATA-1 was incubated with GST-MEK1 bound to glutathione-Sepharose beads, and the binding complex was separated by gel electrophoresis and subjected to autoradiography.

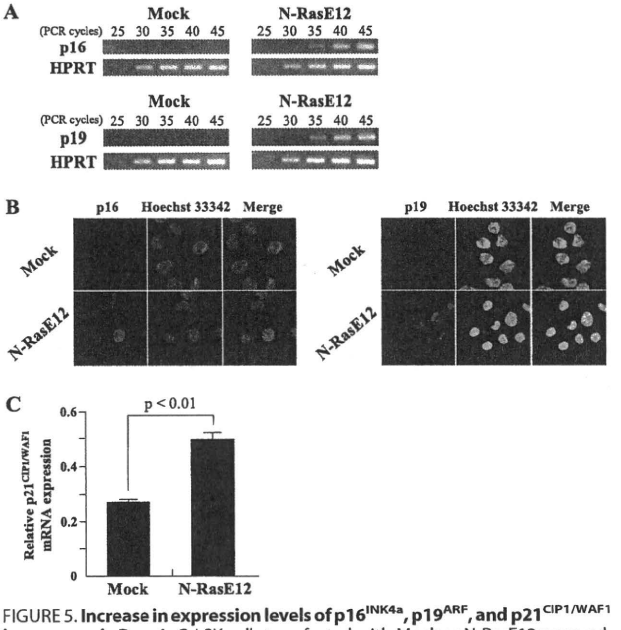

FIGURE 5. **Increase in expression levels of p16^{INK4a}, p19^{ARF}, and p21$^{CIP1/WAF1}$ by oncogenic Ras.** *A–C*, LSK cells transfected with Mock or N-RasE12 were cultured with rmSCF, rmIL-3, and rhEPO for 2 days. Total RNA was isolated from GFP$^+$ cells, and the expression levels of p16^{INK4a} and p19^{ARF} were analyzed by semiquantitative RT-PCR (*A*). Immunofluorescence staining of p16^{INK4a} and p19^{ARF} localizations (*red*) in Hoechst 33342-stained nuclei of GFP$^+$ cells are shown (magnification, 630×) (*B*). The expression levels of p21$^{CIP1/WAF1}$ were analyzed by real-time RT-PCR. The results are normalized to the levels of HPRT gene and shown as means ± S.D. ($n = 3$) (*C*).

because, in myeloid malignancies, N-Ras mutations are more frequent than K-Ras, whereas H-Ras mutations are rare (39, 42–44). It is predictable that activated N-Ras has stronger leukemogenic potential than activated H-Ras or K-Ras.

In contrast to the negative role of oncogenic Ras in erythropoiesis, Ras activation prominently enhanced the development of myeloid cells from LSK cells as observed in CML patients. To clarify the mechanism through which the active form of Ras plays different roles in the growth of hematopoietic cells according to the cell lineages (*i.e.* inhibition of erythropoiesis but promotion of myelopoiesis), we examined the role of GATA-1, which is a transcription factor mainly expressed in erythroid and megakaryocytic cells but not in myeloid cells. Ras-induced suppression of erythropoiesis can be considered to result from inhibition of proliferation of already committed erythroid progenitors, and blockage of commitment into erythroid lineage from HSCs. In this study, we found that GATA-1 inhibits MEK activity and suppresses the Ras-dependent proliferation of GATA-1-posistive cells. GATA-1 is necessary in the post-commitment stages of erythroid and megakaryocytic development, and is highly expressed after the commitment into megakaryocyte-erythrocyte progenitors (MEPs), but is scarcely expressed in HSCs (45). So, it is unlike that the interaction between GATA-1 and MEK1 is associated with the lineage determination of HSCs. On the other hand, recent reports showed that suppression of erythroid cell development by H-, K-, and N-Ras occurs at later stages of differentiation (18, 38, 46). These data are consistent with our result that GATA-1 interacts with MEK1, thereby inhibiting Ras-mediated mitogenic signals.

However, this result raises a question where these molecules interact together in the cells because GATA-1 is located in the nucleus and MEK is in the cytoplasm (47). As an explanation it was previously reported that MEK contains a nuclear export signal in its N-terminal domain, indicating that MEK is translocated to the nucleus upon mitogenic stimulation and then goes back to the cytoplasm after transduction of its signal (48). So, GATA-1 is supposed to interact with MEK1 in the nucleus, thereby inhibiting its activity. This hypothesis that GATA-1 would inhibit MEK activities is also contradictory to the fact that platelet counts are often elevated in CML patients, because MEK has been shown to be important for the maturation (polyploidization) of megakaryocytes, in which GATA-1 is highly expressed as well as in erythroid cells. Regarding this issue, Jacquel *et al.* reported that PMA-induced megakaryocytic maturation is only partly dependent on the MEK/ERK pathway and suggested the involvement of other pathways such

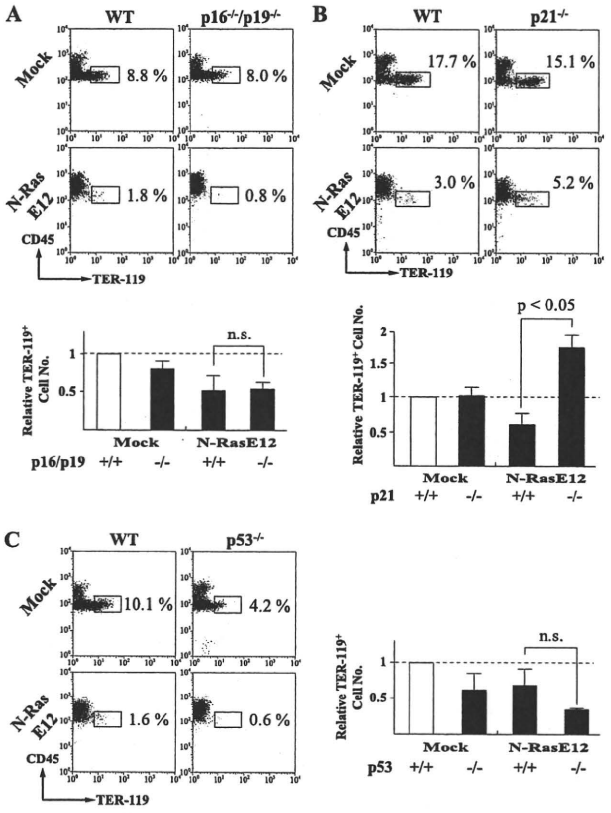

FIGURE 6. **p21$^{CIP1/WAF1}$ but not p53 or p16^{INK4a}/p19^{ARF} mediates oncogenic Ras-induced suppression of erythropoiesis.** *A–C*, LSK cells were isolated from BM of the indicated mice. After retrovirus infection, GFP$^+$ cells were sorted and cocultured with MS-5 in the presence of rmSCF and rhEPO. The expression of CD45 and TER-119 was analyzed after 5 days. Bar graphs represent the relative TER-119$^+$ cell numbers normalized to mock-transduced WT cells (*dashed lines*). *n.s.*, not significant.

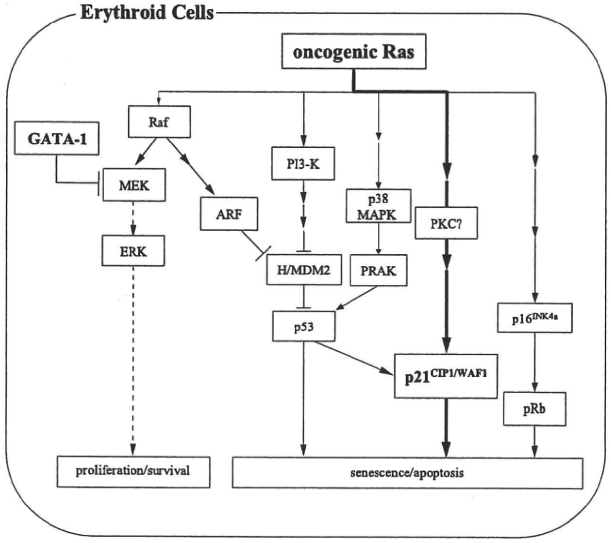

FIGURE 7. **A proposed model for oncogenic Ras-induced suppression of erythropoiesis.** Oncogenic Ras simultaneously activates several downstream molecules including Raf, PI3-K, and p38 MAPK. The Raf/MEK/ERK pathway mainly transduces proliferation and survival signals, while the remaining pathways commonly induce growth arrest (senescence) through cell cycle regulatory molecules such as p16^{INK4a}, p19^{ARF}, p21$^{CIP1/WAF1}$, and p53. So, oncogenic Ras is supposed to induce proliferation or senescence dependently on the balance between these two signals. In this study, we found that GATA-1 inhibits mitogenic signal from Ras through its interaction with MEK1 in erythroid cells, which resulted in their growth inhibition due to the dominance of senescence-inducing signals. In addition, we found that p21$^{CIP1/WAF1}$ is a crucial regulator of oncogenic Ras-induced senescence of erythroid cells.

as Jun N-terminal kinase (JNK) and protein kinase C (PKC) in CML cells (49). Alternatively, it is also possible that the interaction between GATA-1 and MEK might be inhibited in megakaryocytes due to the presence of some nuclear protein(s) specific for this lineage. However, further studies are required to clarify how megakaryocytes develop and platelets are effectively produced in CML patients.

Among various signaling molecules downstream of Ras, the Raf/MEK/ERK pathway mainly promotes cell growth and prevents apoptosis of hematopoietic cells (14). On the other hand, oncogenic stimuli including constitutively activated Ras, also cause growth inhibition (senescence) that acts as a fail-safe mechanism against malignant transformation (15, 16, 21). Although the mechanism of Ras-induced senescence is not fully understood, recent findings have unveiled several MEK/ERK-independent pathways (19). These pathways regulate the function of two main tumor-suppressor molecules, p53 and retinoblastoma protein (pRb) (50). Downstream of oncogenic Ras, p38-regulated/activated protein kinase (PRAK), a substrate of p38 mitogen-activated protein kinase (p38 MAPK), activates p53 by direct phosphorylation (20). Ras/Raf stabilizes p53 independently of MEK through the up-regulation of p19^{ARF} (21). The PI3-K pathway also stabilizes p53 through the inhibition of H/MDM2 (19). So, we speculated that N-RasE12 might induce growth arrest in erythroid cells even if MEK activities are blocked by GATA-1.

Ras-induced senescence is executed by CDK inhibitors such as p16^{INK4a} and p21$^{CIP1/WAF1}$, and a tumor-suppressor, p19^{ARF}, which consequently activate both p53 and pRb pathways. Among these molecules, we here found that p21$^{CIP1/WAF1}$ is a major player of Ras-induced suppression of erythropoiesis (may well be called nearly equal to senescence). Although p21$^{CIP1/WAF1}$ is a transcriptional target of p53 (51), p53 deficiency did not cancel Ras-induced suppression of erythropoiesis. So, p53-independent expression of p21$^{CIP1/WAF1}$ was supposed to be important for Ras-induced suppression of erythropoiesis. Because Darley *et al.* (18) previously showed that oncogenic N-Ras conferred developmental abnormalities on human erythroid cells through the activation of PKC, one of the reported activators of p21$^{CIP1/WAF1}$ (52), PKC may be a candidate molecule involved in Ras-induced expression of p21$^{CIP1/WAF1}$ and consequent suppression of erythropoiesis.

Mutation and/or deletion of the p53 gene and the INK4a/ARF locus are frequently observed in CML blast phase (1), but to our knowledge, there is no report demonstrating the inactivation of the p21$^{CIP1/WAF1}$ gene. So, our findings that p21$^{CIP1/WAF1}$ but not p53 or p16^{INK4a}/p19^{ARF} is the major regulator of Ras-induced suppression of erythropoiesis are again consistent with the clinical features that anemia is continued and erythroid transformation is a rare event in blast-phase

CML (7, 8). Furthermore, because loss-of-function mutations of the p21$^{CIP1/WAF1}$ gene are rare in most of the hematologic malignancies, anemia observed in these diseases might be attributable to p21$^{CIP1/WAF1}$.

In conclusion, we here show that BCR-ABL but not JAK2 V617F inhibits erythropoiesis through the Ras signal. We also identified p21$^{CIP1/WAF1}$ as a central regulator of Ras-induced suppression of erythropoiesis. Ras transmits both growth promoting and inhibitory signals, and then induces proliferation or senescence dependently on their balance. In erythroid but not in myeloid progenitors, the growth promoting signal is inhibited at the level of MEK by GATA-1, which would lead to the relative dominance of the growth inhibitory signal mediated by p21$^{CIP1/WAF1}$ (Fig. 7). These mechanisms would explain why oncogenic Ras simultaneously reveals conflicting effects according to the cell lineage, *i.e.* growth promotion in myeloid cells and growth inhibition in erythroid cells. This model may be also useful to understand the mechanism of anemia caused by other oncogenic TKs.

Acknowledgments—We thank Dr. Connie J. Eaves for providing the vector expressing p210-BCR-ABL, Dr. Kazuya Shimoda for providing the plasmid encoding JAK2 V617F, and Dr. Hiroyuki Miyoshi for providing 293gp cells.

REFERENCES

1. Quintás-Cardama, A., and Cortes, J. (2009) *Blood* **113,** 1619–1630
2. Small, D. (2006) *Hematology Am. Soc. Hematol. Educ. Program,* 178–184
3. Levine, R. L., and Gilliland, D. G. (2008) *Blood* **112,** 2190–2198
4. Ren, R. (2005) *Nat. Rev. Cancer* **5,** 172–183
5. Zeuner, A., Pedini, F., Signore, M., Ruscio, G., Messina, C., Tafuri, A., Girelli, G., Peschle, C., and De Maria, R. (2006) *Blood* **107,** 3495–3502
6. Thiele, J., Kvasnicka, H. M., Schmitt-Graeff, A., Zirbes, T. K., Birnbaum, F., Kressmann, C., Melguizo-Grahmann, M., Frackenpohl, H., Sprungmann, C., Leder, L. D., Diehl, V., Zankovich, R., Schaefer, H. E., Niederle, N., and Fischer, R. (2000) *Leuk. Lymphoma* **36,** 295–308
7. Saikia, T., Advani, S., Dasgupta, A., Ramakrishnan, G., Nair, C., Gladstone, B., Kumar, M. S., Badrinath, Y., and Dhond, S. (1988) *Leuk. Res.* **12,** 499–506
8. Griffin, J. D., Todd, R. F., 3rd, Ritz, J., Nadler, L. M., Canellos, G. P., Rosenthal, D., Gallivan, M., Beveridge, R. P., Weinstein, H., Karp, D., and Schlossman, S. F. (1983) *Blood* **61,** 85–91
9. Sonoyama, J., Matsumura, I., Ezoe, S., Satoh, Y., Zhang, X., Kataoka, Y., Takai, E., Mizuki, M., Machii, T., Wakao, H., and Kanakura, Y. (2002) *J. Biol. Chem.* **277,** 8076–8082
10. Sexl, V., Piekorz, R., Moriggl, R., Rohrer, J., Brown, M. P., Bunting, K. D., Rothammer, K., Roussel, M. F., and Ihle, J. N. (2000) *Blood* **96,** 2277–2283
11. Hoelbl, A., Kovacic, B., Kerenyi, M. A., Simma, O., Warsch, W., Cui, Y., Beug, H., Hennighausen, L., Moriggl, R., and Sexl, V. (2006) *Blood* **107,** 4898–4906
12. Sawyers, C. L., McLaughlin, J., and Witte, O. N. (1995) *J. Exp. Med.* **181,** 307–313
13. Baum, K. J., and Ren, R. (2008) *J. Hematol. Oncol.* **1,** 5
14. Platanias, L. C. (2003) *Blood* **101,** 4667–4679
15. Campisi, J. (2005) *Cell* **120,** 513–522
16. Braig, M., and Schmitt, C. A. (2006) *Cancer Res.* **66,** 2881–2884
17. Darley, R. L., Hoy, T. G., Baines, P., Padua, R. A., and Burnett, A. K. (1997) *J. Exp. Med.* **185,** 1337–1347
18. Darley, R. L., Pearn, L., Omidvar, N., Sweeney, M., Fisher, J., Phillips, S., Hoy, T., and Burnett, A. K. (2002) *Blood* **100,** 4185–4192
19. Yaswen, P., and Campisi, J. (2007) *Cell* **128,** 233–234
20. Sun, P., Yoshizuka, N., New, L., Moser, B. A., Li, Y., Liao, R., Xie, C., Chen, J., Deng, Q., Yamout, M., Dong, M. Q., Frangou, C. G., Yates, J. R., 3rd, Wright, P. E., and Han, J. (2007) *Cell* **128,** 295–308
21. Wahl, G. M., and Carr, A. M. (2001) *Nat. Cell Biol.* **3,** E277–286
22. Ezoe, S., Matsumura, I., Gale, K., Satoh, Y., Ishikawa, J., Mizuki, M., Takahashi, S., Minegishi, N., Nakajima, K., Yamamoto, M., Enver, T., and Kanakura, Y. (2005) *J. Biol. Chem.* **280,** 13163–13170
23. Delgado, M. D., Vaqué, J. P., Arozarena, I., López-Ilasaca, M. A., Martínez, C., Crespo, P., and León, J. (2000) *Oncogene* **19,** 783–790
24. Onishi, M., Nosaka, T., Misawa, K., Mui, A. L., Gorman, D., McMahon, M., Miyajima, A., and Kitamura, T. (1998) *Mol. Cell. Biol.* **18,** 3871–3879
25. Egawa, K., Sharma, P. M., Nakashima, N., Huang, Y., Huver, E., Boss, G. R., and Olefsky, J. M. (1999) *J. Biol. Chem.* **274,** 14306–14314
26. Jiang, X., Ng, E., Yip, C., Eisterer, W., Chalandon, Y., Stuible, M., Eaves, A., and Eaves, C. J. (2002) *Blood* **100,** 3731–3740
27. Shide, K., Shimoda, H. K., Kumano, T., Karube, K., Kameda, T., Takenaka, K., Oku, S., Abe, H., Katayose, K. S., Kubuki, Y., Kusumoto, K., Hasuike, S., Tahara, Y., Nagata, K., Matsuda, T., Ohshima, K., Harada, M., and Shimoda, K. (2008) *Leukemia* **22,** 87–95
28. Matsumura, I., Kanakura, Y., Kato, T., Ikeda, H., Horikawa, Y., Ishikawa, J., Kitayama, H., Nishiura, T., Tomiyama, Y., Miyazaki, H., and Matsuzawa, Y. (1996) *Blood* **88,** 3074–3082
29. Fukushima, K., Matsumura, I., Ezoe, S., Tokunaga, M., Yasumi, M., Satoh, Y., Shibayama, H., Tanaka, H., Iwama, A., and Kanakura, Y. (2009) *J. Biol. Chem.* **284,** 7719–7732
30. Roussel, M. F. (1999) *Oncogene* **18,** 5311–5317
31. el-Deiry, W. S., Tokino, T., Velculescu, V. E., Levy, D. B., Parsons, R., Trent, J. M., Lin, D., Mercer, W. E., Kinzler, K. W., and Vogelstein, B. (1993) *Cell* **75,** 817–825
32. Macleod, K. F., Sherry, N., Hannon, G., Beach, D., Tokino, T., Kinzler, K., Vogelstein, B., and Jacks, T. (1995) *Genes Dev.* **9,** 935–944
33. Parker, S. B., Eichele, G., Zhang, P., Rawls, A., Sands, A. T., Bradley, A., Olson, E. N., Harper, J. W., and Elledge, S. J. (1995) *Science* **267,** 1024–1027
34. Khalaf, W. F., White, H., Wenning, M. J., Orazi, A., Kapur, R., and Ingram, D. A. (2005) *Blood* **105,** 3538–3541
35. Sui, X., Krantz, S. B., You, M., and Zhao, Z. (1998) *Blood* **92,** 1142–1149
36. Esteban, L. M., Vicario-Abejón, C., Fernández-Salguero, P., Fernández-Medarde, A., Swaminathan, N., Yienger, K., Lopez, E., Malumbres, M., McKay, R., Ward, J. M., Pellicer, A., and Santos, E. (2001) *Mol. Cell. Biol.* **21,** 1444–1452
37. Umanoff, H., Edelmann, W., Pellicer, A., and Kucherlapati, R. (1995) *Proc. Natl. Acad. Sci. U.S.A.* **92,** 1709–1713
38. Zhang, J., Socolovsky, M., Gross, A. W., and Lodish, H. F. (2003) *Blood* **102,** 3938–3946
39. MacKenzie, K. L., Dolnikov, A., Millington, M., Shounan, Y., and Symonds, G. (1999) *Blood* **93,** 2043–2056
40. Metcalfe, D. D. (2008) *Blood* **112,** 946–956
41. Wheadon, H., and Welham, M. J. (2003) *Blood* **102,** 1480–1489
42. Döhner, K., and Döhner, H. (2008) *Haematologica* **93,** 976–982
43. Neubauer, A., Greenberg, P., Negrin, R., Ginzton, N., and Liu, E. (1994) *Leukemia* **8,** 638–641
44. Flotho, C., Valcamonica, S., Mach-Pascual, S., Schmahl, G., Corral, L., Ritterbach, J., Hasle, H., Aricò, M., Biondi, A., and Niemeyer, C. M. (1999) *Leukemia* **13,** 32–37
45. Akashi, K., Traver, D., Miyamoto, T., and Weissman, I. L. (2000) *Nature* **404,** 193–197
46. Zhang, J., Liu, Y., Beard, C., Tuveson, D. A., Jaenisch, R., Jacks, T. E., and Lodish, H. F. (2007) *Blood* **109,** 5238–5241
47. Lenormand, P., Sardet, C., Pagès, G., L'Allemain, G., Brunet, A., and Pouysségur, J. (1993) *J. Cell Biol.* **122,** 1079–1088
48. Jaaro, H., Rubinfeld, H., Hanoch, T., and Seger, R. (1997) *Proc. Natl. Acad. Sci. U.S.A.* **94,** 3742–3747
49. Jacquel, A., Herrant, M., Defamie, V., Belhacene, N., Colosetti, P., Marchetti, S., Legros, L., Deckert, M., Mari, B., Cassuto, J. P., Hofman, P., and Auberger, P. (2006) *Oncogene* **25,** 781–794
50. Serrano, M., Lin, A. W., McCurrach, M. E., Beach, D., and Lowe, S. W. (1997) *Cell* **88,** 593–602
51. Deng, Y., Chan, S. S., and Chang, S. (2008) *Nat. Rev. Cancer* **8,** 450–458
52. Biggs, J. R., Kudlow, J. E., and Kraft, A. S. (1996) *J. Biol. Chem.* **271,** 901–906

Letter to the Editor

Auto- and cross-induction by betacellulin in epidermal keratinocytes

To the Editor,

Keratinocytes comprise the main cellular component of the epidermis. Their growth is regulated by both positive and negative mediators [1]. Among the most important stimulators of keratinocyte proliferation are members of the epidermal growth factor (EGF) family, which comprises EGF, transforming growth factor (TGF)-α, heparin-binding EGF-like growth factor (HB-EGF), amphiregulin (AREG), epiregulin (EREG), betacellulin (BTC), and neuregulin 1–4 [2]. EGF receptors include ErbB1 (universally referred to as EGFR), ErbB2, ErbB3 and ErbB4. EGF family members may be classified according to their receptor binding capacities. EGF, TGF-α and AREG bind to ErbB1, while HB-EGF, EREG and BTC bind to both ErbB1 and ErbB4.

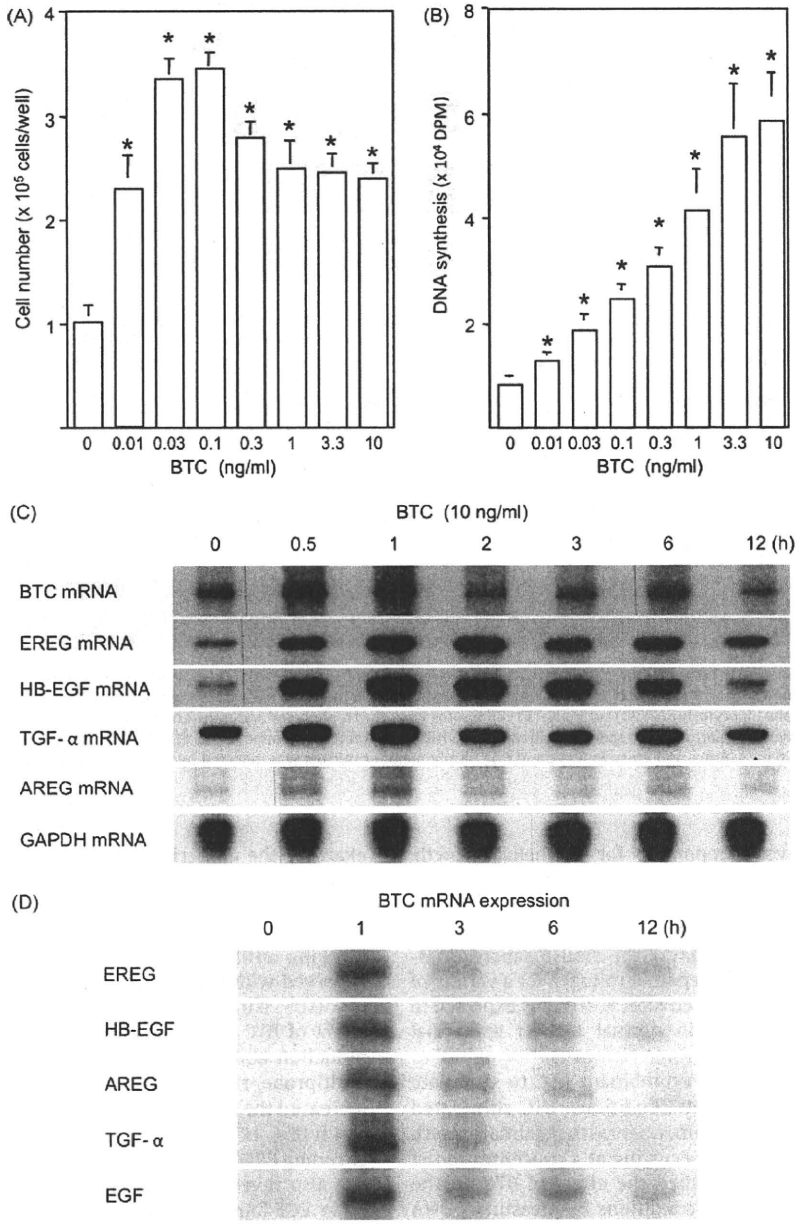

Fig. 1. Effects of BTC on the proliferation of human epidermal keratinocytes. (A) Keratinocytes were seeded to 6-well plates at a density of 2×10^4 cells/well. The next day, the cells were re-fed with fresh medium containing various concentrations of recombinant BTC. Four days later, cells were counted using a hemocytometer. (B) Various concentrations of BTC were added to the medium under confluent conditions. After 24 h, DNA synthesis was measured by ^{3}H-thymidine uptake. Asterisks show a significant difference ($p < 0.01$) from the corresponding control (no BTC). (C) Confluent keratinocytes were incubated with 10 ng/ml BTC or (D) EGF, HB-EGF, EREG, TGF-α and EGF (each at a concentration of 2 nM). Total RNA was extracted at the indicated time points. EGF family mRNA expression was analyzed by multiprobe ribonuclease protection assay.

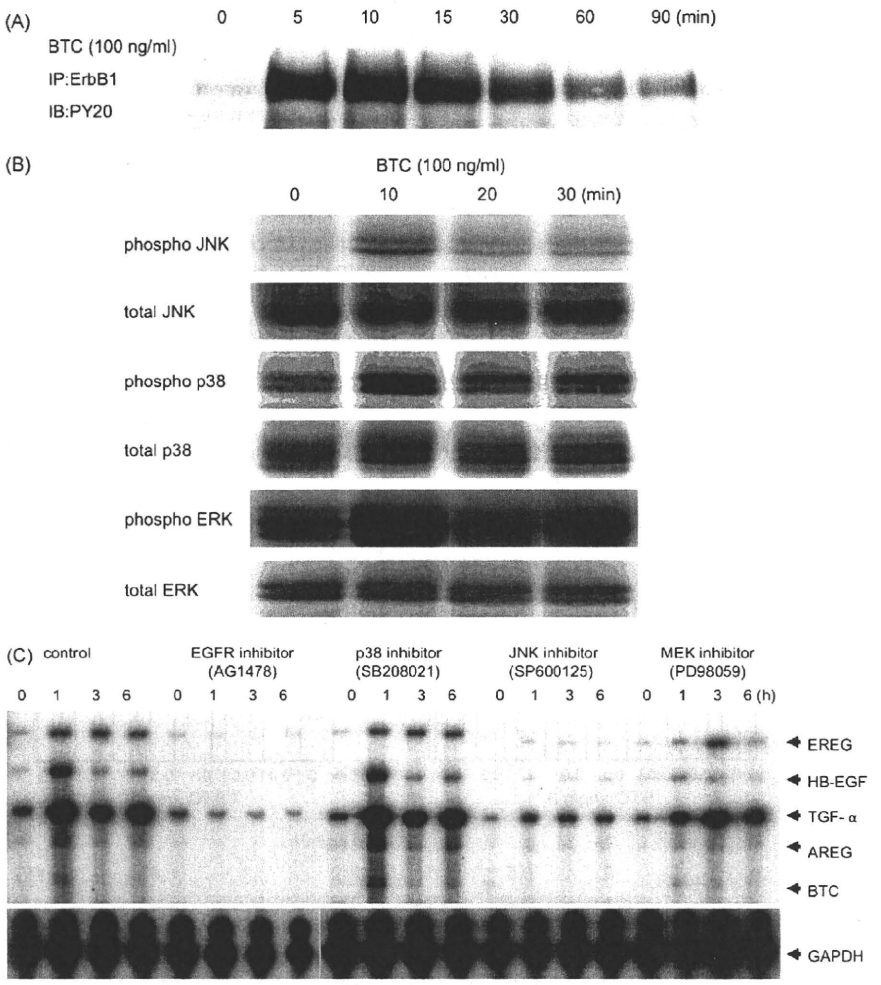

Fig. 2. Involvement of BTC in signal transduction pathway, auto- and cross-induction. (A) Keratinocytes were treated with BTC (100 ng/ml). Cell lysates were immunoprecipitated with an anti-ErbB1 antibody and separated on a 7.5% acrylamide gel by SDS-PAGE. Following transfer to a nitrocellulose membrane, phosphorylated ErbB1 was detected with anti-phosphotyrosine (PY20) antibody. (B) Cell lysates were electrophoresed and transferred to nitrocellulose membrane. Phosphorylation of ERK, p38 and JNK were detected by Western blotting using specific antibodies. (C) NHEK were treated with inhibitors of ErbB1, ERK, p38 and JNK for 1 h prior to BTC treatment. RNA was harvested at several time points. Auto- and cross-induction of EGF family member mRNAs was detected by multiprobe ribonuclease protection assay.

ErbB1 signaling is very important for epithelial growth. Previous reports have shown that TGF-α, HB-EGF, AREG and EREG synthesized and secreted by keratinocytes act as autocrine growth factors [1,3]. BTC was initially purified as a growth-promoting factor from the conditioned medium of the mouse pancreatic β-cell carcinoma cell line [4]. BTC is a potent mitogen for a variety of cell types [4]. Since BTC binds and activates ErbB1, it is expected to be an autocrine growth factor in normal human epidermal keratinocytes (NHEK).

We first tested the ability of recombinant BTC to stimulate NHEK growth under sub-confluent conditions. BTC stimulated NHEK growth in a dose-dependent manner, with maximal growth stimulation (3.5-fold vs. control) occurring at a concentration of 0.1 ng/ml (Fig. 1A). Next, we studied the effect of BTC on the growth of NHEK under confluent conditions by measuring DNA synthesis. In contrast to its effects on sub-confluent cells, BTC dose-dependently stimulated NHEK proliferation up to a concentration of 10 ng/ml (Fig. 1B). These proliferative effects are thus dependent on cell density, and the effective dose is higher in confluent conditions than in sub-confluent conditions. To examine the autocrine action of BTC in NHEK, we determined the effect of an anti-BTC blocking antibody on NHEK growth. Sub-confluent NHEK were re-fed with fresh medium containing anti-BTC antibody (10 μg/ml) or normal goat IgG (10 μg/ml). The blocking antibody reduced DNA synthesis to 80% of the level observed with normal rabbit IgG after a 24 h incubation period ($p < 0.05$, data not shown). This result indicates the autocrine effect of BTC on NHEK growth. To clarify the auto- and cross-induction ability of BTC, we investigated mRNA expression. A multiprobe ribonuclease protection assay revealed that BTC increased the levels of BTC mRNA, with peak induction occurring at 1 h (Fig. 1C). BTC also increased the expression of the mRNAs encoding EREG, HB-EGF, TGF-α and AREG (peak induction at 1 h). We also investigated whether BTC expression is enhanced by other EGF family growth factors. EGF, EREG, HB-EGF, AREG and TGF-α (each at a concentration of 2 nM) increased the expression of BTC mRNA at 1 h (Fig. 1D). These results indicate that BTC is an autocrine growth factor in NHEK that, along with HB-EGF, AR, TGF-α and EREG, forms auto- and cross-induction regulatory networks during NHEK growth.

We also investigated the signal transduction pathways involved in BTC auto- and cross-induction. Western blot analysis showed that BTC activates ErbB1 in NHEK (Fig. 2A). A previous report showed that BTC activates mitogen activated protein kinase (MAPK). We examined whether BTC activates MAPK proteins in NHEK. BTC stimulated the phosphorylation of MAPK proteins including extracellular signal-regulated kinase (ERK), p38, and c-Jun N-terminal kinase (JNK) in NHEK (Fig. 2B). To examine which pathways might be involved in auto- and cross-induction, we used specific inhibitors of ErbB1, MAKP/ERK kinase (MEK, upstream of ERK), p38 and JNK. Treatment with the ErbB1 inhibitor completely blocked the induction of BTC, as well as other EGF family members, while treatment with the JNK and MEK inhibitors suppressed their expression (Fig. 2C). By contrast, the p38 inhibitor did not affect the induction of EGF family members by BTC (Fig. 2C). These results indicate that BTC induces auto- and cross-induction through the activation of ErbB1, MEK-ERK, and JNK signaling. The effect of MEK inhibitor is less effective than ErbB1 inhibitor or JNK inhibitor. Because knockout of MAPK pathways leads to distinct phenotypes in mice [5], the differences of the effects on auto- and cross-induction may be due to their specific non-redundant biological functions.

This study directly demonstrates that BTC, like HB-EGF, AREG, TGF-α and EREG, is an autocrine growth factor in NHEK. All EGF family members that bind ErbB1 promote NHEK growth. However, they each have their own distinct biological functions. Loss of TGF-α *in vivo* results in the retardation of partial thickness wound healing. In keratinocyte-specific HB-EGF knockout mice, the migration but not proliferation of wound edge keratinocytes was impaired [6]. Loss of other EGF family members causes no obvious skin phenotype in mice. AREG-transgenic mice exhibited a severe inflammatory and hyperproliferative psoriatic phenotype, while TGF-α overexpression causes epidermal thickening [7,8]. By contrast, BTC-transgenic mice showed increased keratinocyte proliferation, a significant delay in hair follicle morphogenesis, and enhanced wound healing-associated angiogenesis [9]. Immunohistochemical staining revealed that HB-EGF was diffusely expressed throughout normal and psoriatic epidermis, whereas BTC was largely restricted to the spinous and granular layer [10]. These findings suggest that BTC, like other autocrine growth factors, may have a distinct, non-redundant biological function in normal human skin.

We have shown that BTC induces its own expression, as well as that of other EGF family members, and that other EGF family members induce BTC expression. Auto- and cross-regulatory mechanisms may be very effective in stimulating keratinocyte proliferation, but problematic when the aim is to arrest tumor cell growth. We clearly demonstrated that auto- and cross-induction are mediated through ErbB1, MEK-ERK, and JNK pathways. Numerous ErbB blockers have been tested as possible suppressors of tumor growth and some, including anti-ErbB1 monoclonal antibodies and tyrosine kinase inhibitors, are now being used clinically [2]. Therapeutic strategies targeting MEK-ERK or JNK, meanwhile, may produce beneficial anti-proliferative effects in hyperproliferative disorders of the epidermis.

In this study, we demonstrate that BTC is an autocrine growth factor in NHEK and that auto- and cross-induction of EGF family members by BTC is mediated by the ERK and JNK signaling pathways.

Acknowledgements

This work was supported by a Grant-in-aid for Scientific Research from the Ministry of Education, Science, Culture and Sports of Japan, and by Health and Labour Sciences Research Grants (Research on Intractable Diseases) from the Ministry of Health, Labour and Welfare of Japan.

References

[1] Hashimoto K. Regulation of keratinocyte function by growth factors. J Dermatol Sci 2000;24(Suppl 1):S46–50.
[2] Kataoka H. EGFR ligands and their signaling scissors, ADAMs, as new molecular targets for anticancer treatments. J Dermatol Sci 2009;56:148–53.
[3] Shirakata Y, Komurasaki T, Toyoda H, Hanakawa Y, Yamasaki K, Tokumaru S, et al. a novel member of the epidermal growth factor family, is an autocrine growth factor in normal human keratinocytes. J Biol Chem 2000;275:5748–53.
[4] Dunbar AJ, Goddard C. Structure-function and biological role of betacellulin. Int J Biochem Cell Biol 2000;32:805–15.
[5] Aouadi M, Binetruy B, Caron L, Le Marchand-Brustel Y, Bost F. Role of MAPKs in development and differentiation: lessons from knockout mice. Biochimie 2006;88:1091–8.
[6] Shirakata Y, Kimura R, Nanba D, et al. Heparin-binding EGF-like growth factor accelerates keratinocyte migration and skin wound healing. J Cell Sci 2005;118:2363–70.
[7] Cook PW, Piepkorn M, Clegg CH, Plowman GD, DeMay JM, Brown JR, et al. Transgenic expression of the human amphiregulin gene induces a psoriasis-like phenotype. J Clin Invest 1997;100:2286–94.
[8] Vassar R, Fuchs E. Transgenic mice provide new insights into the role of TGF-alpha during epidermal development and differentiation. Genes Dev 1991;5: 714–27.
[9] Schneider MR, Antsiferova M, Feldmeyer L, Dahlhoff M, Bugnon P, Hasse S, et al. Betacellulin regulates hair follicle development and hair cycle induction and enhances angiogenesis in wounded skin. J Invest Dermatol 2008;128:1256–65.
[10] Piepkorn M, Predd H, Underwood R, Cook P. Proliferation-differentiation relationships in the expression of heparin-binding epidermal growth factor-related factors and erbB receptors by normal and psoriatic human keratinocytes. Arch Dermatol Res 2003;295:93–101.

Yuji Shirakata*
Sho Tokumaru
Koji Sayama
Koji Hashimoto
Department of Dermatology, Ehime University Graduate School of Medicine, Shitsukawa, Toon, Ehime 791-0295, Japan
*Corresponding author. Tel.: +81 89 960 5350; fax: +81 89 960 5352

E-mail address: shirakat@m.ehime-u.ac.jp (Y. Shirakata)

4 March 2010

doi:10.1016/j.jdermsci.2010.03.016

Inflammatory Mediator TAK1 Regulates Hair Follicle Morphogenesis and Anagen Induction Shown by Using Keratinocyte-Specific TAK1-Deficient Mice

Koji Sayama[1]*, Kentaro Kajiya[2], Koji Sugawara[3], Shintaro Sato[4], Satoshi Hirakawa[1], Yuji Shirakata[1], Yasushi Hanakawa[1], Xiuju Dai[1], Yumiko Ishimatsu-Tsuji[2], Daniel Metzger[5], Pierre Chambon[5], Shizuo Akira[6], Ralf Paus[3,7], Jiro Kishimoto[2], Koji Hashimoto[1]

1 Department of Dermatology, Ehime University Graduate School of Medicine, Ehime, Japan, 2 Skin Biology Research Group, Shiseido Innovative Science Research and Development Center, Yokohama, Japan, 3 Department of Dermatology, University of Luebeck, Luebeck, Germany, 4 Department of Microbiology and Immunology, The Institute of Medical Science, The University of Tokyo, Tokyo, Japan, 5 Institut de Génétique et de Biologie Moléculaire et Cellulaire (IGBMC), CNRS, INSERM, UdS, Collège de France, Illkirch, France, 6 Research Institute for Microbial Disease, Osaka University, Suita, Japan, 7 School of Translational Medicine, University of Manchester, Manchester, United Kingdom

Abstract

Transforming growth factor-β-activated kinase 1 (TAK1) is a member of the NF-κB pathway and regulates inflammatory responses. We previously showed that TAK1 also regulates keratinocyte growth, differentiation, and apoptosis. However, it is unknown whether TAK1 has any role in epithelial–mesenchymal interactions. To examine this possibility, we studied the role of TAK1 in mouse hair follicle development and cycling as an instructive model system. By comparing keratinocyte-specific TAK1-deficient mice (*Map3k7*$^{fl/fl}$K5-Cre) with control mice, we found that the number of hair germs (hair follicles precursors) in *Map3k7*$^{fl/fl}$K5-Cre mice was significantly reduced at E15.5, and that subsequent hair follicle morphogenesis was retarded. Next, we analyzed the role of TAK1 in the cyclic remodeling in follicles by analyzing hair cycle progression in mice with a tamoxifen-inducible keratinocyte-specific TAK1 deficiency (*Map3k7*$^{fl/fl}$K14-Cre-ER^{T2}). After active hair growth (anagen) was induced by depilation, TAK1 was deleted by topical tamoxifen application. This resulted in significantly retarded anagen development in TAK1-deficient mice. Deletion of TAK1 in hair follicles that were already in anagen induced premature, apoptosis-driven hair follicle regression, along with hair follicle damage. These studies provide the first evidence that the inflammatory mediator TAK1 regulates hair follicle induction and morphogenesis, and is required for anagen induction and anagen maintenance.

Citation: Sayama K, Kajiya K, Sugawara K, Sato S, Hirakawa S, et al. (2010) Inflammatory Mediator TAK1 Regulates Hair Follicle Morphogenesis and Anagen Induction Shown by Using Keratinocyte-Specific TAK1-Deficient Mice. PLoS ONE 5(6): e11275. doi:10.1371/journal.pone.0011275

Editor: Vincent Laudet, Ecole Normale Supérieure de Lyon, France

Received March 19, 2010; **Accepted** May 30, 2010; **Published** June 23, 2010

Funding: This study was supported in part by grants from the Ministries of Education, Culture, Sports, Science, and Technology of Japan to K.S. and K.H., by Health and Labor Sciences Research Grants (Research on Intractable Diseases) from the Ministry of Health, Labor, and Welfare of Japan to K.H., by the Deutsche Forschungsgemeinschaft (DFG 345 Pa/12-2) to R.P., and by the College de France to P.C. The funders had no role in study design, data collection and analysis, decision to publish, or preparation of the manuscript.

Competing Interests: The authors have declared that no competing interests exist.

* E-mail: sayama@m.ehime-u.ac.jp

Introduction

The NF-κB pathway mediates innate immune or pro-inflammatory responses, such as signaling by Toll-like receptors (TLRs), the IL-1 receptor (IL-1R), and tumor necrosis factor receptor (TNFR) [1,2]. Transforming growth factor-β-activated kinase 1 (TAK1) is a member of the MAP3 kinase family [3] and an important member of the NK-κB pathway, involved in IL-1 and TNF-α-induced activation of NF-κB and MAP kinases [1]. Upon ligand binding, TNF-receptor-associated factor (TRAF) 6 or TRAF2 [4,5,6] activates TAK1, which then phosphorylates IκB kinases (IKKs), resulting in NF-κB activation.

Because members of the NF-κB pathway are increasingly recognized as important in the regulation of epithelial–mesenchymal interaction systems, ranging from tooth development to hair follicle induction and morphogenesis [7,8,9,10,11], we were interested in learning whether TAK1 also played a role in the biology of the hair follicle, a prototypic epithelial–mesenchymal interaction system. This interest was further fueled by our previous discovery in keratinocyte-specific TAK1-deficient mice (*Map3k7*$^{fl/fl}$K5-Cre) that TAK1 regulates keratinocyte growth, differentiation, and apoptosis [12]. However, the role of TAK1 in hair follicles has not been previously studied.

Induction and morphogenesis of the hair follicle [13] is controlled by complex signaling networks within the skin epithelium and between the epithelium and specialized inductive fibroblasts in its adjacent mesenchyme [7,11]. Among these signaling networks, the NF-κB pathway and Wnt/β-catenin signaling provide central controls [7,8]; however, the exact relationship between these signaling networks is not fully understood. Binding of EdaA1 to its receptor EdaR in the embryo is essential for the development of ectodermal appendages [14], and mutations in these genes cause reduced or absent ectodermal appendages [15,16,17,18,19]. Subsequently, the EdaA1/EdaR pathway activates the downstream NF-κB pathway [20]. A recent report showed that Wnt/β-catenin signaling lies both upstream

and downstream of the EdaR/NF-κB pathway [8]. Wnt/β-catenin signaling within the epithelial cells is required for activation of the Eda/EdaR/NF-κB pathway at an early stage of hair follicle development [8], and the expression of Eda and EdaR requires Wnt/β-catenin signaling [8]. At a later stage, maintenance of Wnt signaling and elevated Wnt10a, Wnt10b, and Dkk4 expression requires the Eda/EdaR/NF-κB pathway [8].

The postnatal hair cycle in mice begins with catagen induction around P17, followed by the first telogen. Recently, the EdaR pathway has been shown to be involved in the hair cycle [9,21,22]. The expression of EdaA1 and EdaR increases in the anagen-catagen phase [21]. Furthermore, EdaA1 prolongs the anagen phase [22]. Thus, in addition to its well-established role in hair follicle morphogenesis, the EdaR pathway is also involved in hair cycle control.

Since TAK1 is a member of NF-κB pathway, we hypothesized that TAK1 is involved in hair follicle morphogenesis and hair cycle control. To explore this, we studied hair follicle development in keratinocyte-specific TAK1-deficient (*Map3k7*$^{fl/fl}$K5-Cre) mice and subsequent hair follicle cycling in tamoxifen-inducible keratinocyte-specific TAK1 deficient mice (*Map3k7*$^{fl/fl}$K14-Cre-ER^{T2}) to avoid gene-targeting in embryonic development because this might damage the hair follicle, impairing its later capacity to cycle. These studies provide the first evidence that TAK1 regulates hair follicle induction, morphogenesis, and cycling.

Materials and Methods

Ethics Statement

The protocol for generating *Map3k7*$^{fl/fl}$K5-Cre mice and *Map3k7*$^{fl/fl}$K14-Cre-ER^{T2} mice was approved by the Institutional Review Board of Ehime University Graduate School of Medicine (#I-20-13 and #NE-27-16).

Generation of keratinocyte-specific TAK1-deficient mice (*Map3k7*$^{fl/fl}$ K5-Cre)

TAK1 is encoded by the *Map3k7* gene. The targeting construct has been described previously [1]. We generated keratinocyte-specific TAK1-deficient mice (*Map3k7*$^{fl/fl}$K5-Cre) by breeding *Map3k7*$^{fl/fl}$ mice (C57Bl/6 background) with K5-Cre mice (C57Bl/6 background) [23], as previously described [12].

Generation of tamoxifen-inducible keratinocyte-specific TAK1-deficient mice (*Map3k7*$^{fl/fl}$ K14-Cre-ER^{T2})

Map3k7K$^{fl/fl}$ mice were bred with K14-Cre-ER^{T2} mice (C57Bl/6 background) [24,25] to generate *Map3k7*$^{fl/fl}$K14-Cre-ER^{T2} mice. We applied 100 μL of 4-hydroxytamoxifen (Sigma-Aldrich Co., St. Louis, MO) in ethanol at a concentration of 1 mg/mL topically to the dorsal skin of 8-week-old female *Map3k7*$^{fl/fl}$K14-Cre-ER^{T2} mice for 5 consecutive days [24].

Wax depilation

The hair cycle was synchronized in the dorsal skin of 8-week-old female mice by wax (SURGI-WAX^{TM}, Ardell International, Los Angeles, CA) depilation, as described previously [26].

Histological analysis

The stages of hair follicle morphogenesis, cycling, and dystrophic catagen were morphologically defined using dorsal skin of the mice and the score was defined as follows.

The hair morphogenesis stage of each hair follicle in each mouse group was evaluated as described previously [13]. At least 40 hair follicles or all hair follicles in the mice were evaluated in each mouse group (two mice/group). The score of each hair morphogenesis stage was defined as follows: stage 1 = 1, stage 2 = 2, stage 3 = 3, stage 4 = 4, stage 5 = 5, stage 6 = 6, stage 7 = 7, and stage 8 = 8. Then, the rate (%) of a certain hair morphogenesis stage in the total hair follicles and the median score in each mouse group were determined. The score of *Map3k7*$^{fl/fl}$K5-Cre mice was compared with *Map3k7*$^{fl/fl}$ mice. Statistical significance was determined using a Mann-Whitney's U-test. A difference of $*P<0.01$ was considered statistically significant.

The hair cycle stage of each hair follicle in each mouse group was evaluated as described previously [27]. At least 40 hair follicles were evaluated in each mouse group (two mice/group). The score of each hair cycle stage was defined as follows: catagen I = 1, catagen II = 2, catagen III = 3, catagen IV = 4, catagen V = 5, catagen VI = 6, catagen VII = 7, catagen VIII = 8, telogen = 9, anagen I = 10, anagen II = 11, anagen IIIa = 12, anagen IIIb = 13, anagen IIIc = 14, anagen IV = 15, anagen V = 16, and anagen VI = 17. Then, the rate (%) of a certain hair cycle stage in the total hair follicles and the median score in each mouse group were determined. The score of tamoxifen-treated *Map3k7*$^{fl/fl}$K14-Cre-ER^{T2} mice was compared with the control mice. Statistical significance was determined using a Mann-Whitney's U-test. A difference of $*P<0.01$ was considered statistically significant.

Dystrophic catagen was defined according to a previous report [28] as early dystrophic catagen, mid dystrophic catagen, late dystrophic catagen, and dystrophic telogen. Then, the rate (%) of a certain hair follicle stage per total hair follicles was calculated in each mouse group. At least 40 hair follicles were evaluated in each mouse group (two mice/group).

Results

Impaired hair follicle morphogenesis in keratinocyte-specific TAK1-deficient mice

Keratinocyte-specific TAK1-deficient (*Map3k7*$^{fl/fl}$K5-Cre) mice were generated, as previously described [12]. *Map3k7*$^{fl/fl}$ mice were used as controls. Histological analysis of hair follicle development is shown in Figure 1A. Although hair germs (follicle precursors) and dermal condensations appeared in both types of mice at E15.5, the number of hair germs in *Map3k7*$^{fl/fl}$K5-Cre mice was significantly lower than that in *Map3k7*$^{fl/fl}$ mice (Fig. 1A). At E16.5, the hair germ further progressed into the hair peg stage of hair follicle morphogenesis in *Map3k7*$^{fl/fl}$ mice at the rate expected for wild-type mice [29], while hair pegs were essentially absent in *Map3k7*$^{fl/fl}$K5-Cre mice. Similarly, at P1-6, postnatal hair follicle development was severely impaired in *Map3k7*$^{fl/fl}$K5-Cre mice (Fig. 1A).

Hair follicle morphogenesis was quantitatively analyzed. The morphogenesis stage and the median score of each mouse group are shown in Fig. 1B. Hair follicle morphogenesis indicators were significantly delayed in *Map3k7*$^{fl/fl}$K5-Cre mice, as evident from their lower hair morphogenesis score, compared with *Map3k7*$^{fl/fl}$ mice at P3 and P6 (Fig. 1B).

Generation of tamoxifen-inducible keratinocyte-specific TAK1-deficient mice

Because germline targeting of TAK1 greatly disrupted hair morphogenesis and, thus, precluded a meaningful analysis of subsequent hair follicle cycling, we next used tamoxifen-inducible keratinocyte-specific TAK1-deficient mice (*Map3k7*$^{fl/fl}$K14-Cre-ER^{T2}), in which Cre-ER^{T2} was expressed in the epidermis under the control of the K14 promoter [24]. Southern blot analysis demonstrated efficient deletion of the floxed allele in the epidermis of tamoxifen-treated *Map3k7*$^{fl/fl}$K14-Cre-ER^{T2} mice (Fig. 2).

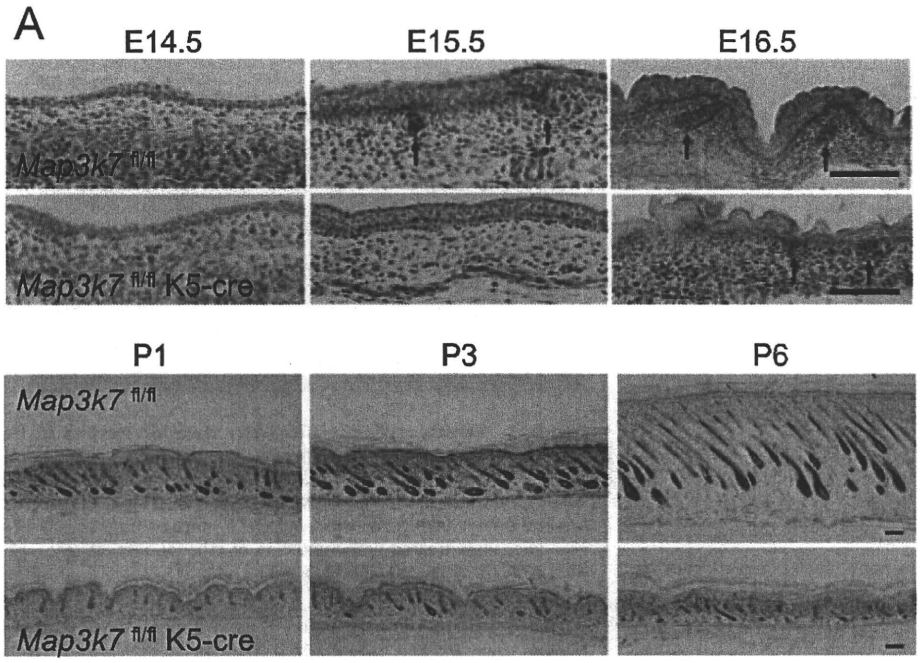

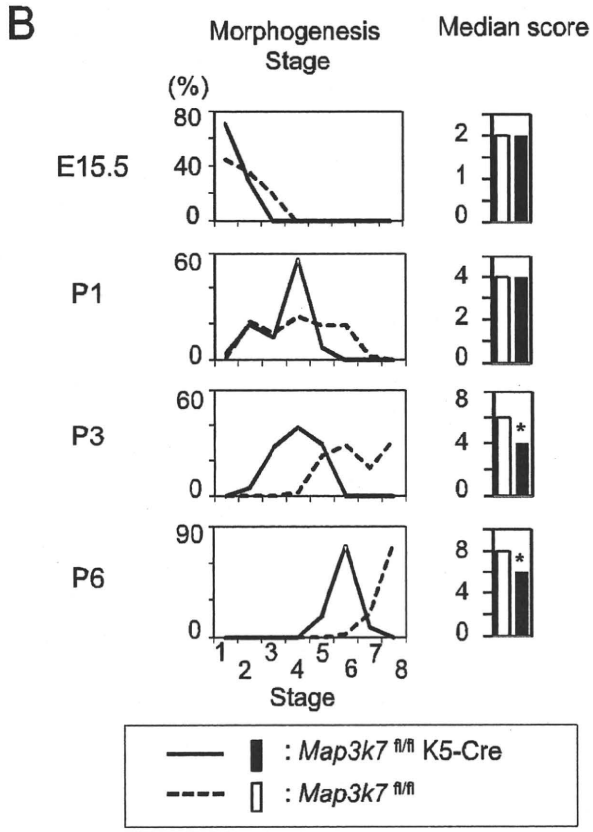

Figure 1. Impaired hair follicle morphogenesis in keratinocyte-specific TAK1-deficient mice. (A) Histological analysis of hair follicle development from E14.5 to P6. *Map3k7*$^{fl/fl}$K5-Cre were keratinocyte-specific TAK1-deficient mice [12]. *Map3k7*$^{fl/fl}$ mice were used as controls. Arrows indicate hair germs or hair pegs. Scale bar, 100 μm. (B) The hair morphogenesis stage of each hair follicle in each mouse group was evaluated as described previously [13]. Then, the rate (%) of a certain hair morphogenesis stage in the total hair follicles (left panel) and the median score in each mouse group (right panel) were determined. The score of *Map3k7*$^{fl/fl}$K5-Cre mice was compared with *Map3k7*$^{fl/fl}$ mice. Statistical significance was determined using a Mann-Whitney's U-test. *$P<0.01$.
doi:10.1371/journal.pone.0011275.g001

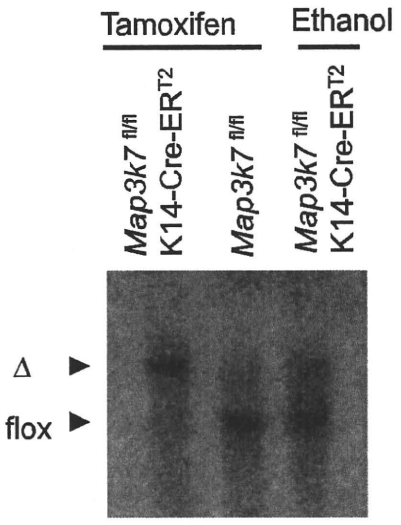

Figure 2. Southern blot analysis. Genomic DNA prepared from the ear skin of mice treated with tamoxifen solution (15 μL/ear) or ethanol for 5 consecutive days was digested with *Xba*I and *Eco*RI. Southern blot analysis for the deletion of the floxed *Tak1* allele was performed as described previously [1]. Cre expression resulted in excision of the floxed allele (*flox*) and generated the deleted allele (Δ) of *Map3k7*.
doi:10.1371/journal.pone.0011275.g002

Although, the skin sample for Southern blot analysis contained non-keratinocyte cells, such as Langerhans cells, melanocytes, or fibroblasts, the band of tamoxifen-treated *Map3k7*$^{fl/fl}$K14-Cre-ER^{T2} mice was a single-recombined band. Since, the majority of this skin sample consists of keratinocytes, flox band of non-keratinocyte cells may not be apparent in this blot. Ethanol-treated *Map3k7*$^{fl/fl}$K14-Cre-ER^{T2} mice also show a minor recombination band, presumably due to slightly leaky Cre- ER^{T2} activity.

Keratinocyte-specific TAK1 deletion results in hair loss in adolescent mice

In the first experiment, tamoxifen was simply applied to the dorsal skin of 8 weeks old mice for 5 consecutive days. Two weeks after the application, the tamoxifen-treated *Map3k7*$^{fl/fl}$K14-Cre-ER^{T2} mice started to lose their hair shafts, and this process continued for more than 4 weeks (Fig. 3). This phenotype suggested the involvement of TAK1 in hair follicle cycling.

Keratinocyte-specific TAK1 deletion delays hair cycle progression in adolescent mice

To further dissect the role of TAK1 in hair follicle cycling, synchronized, active hair growth (anagen) was induced in resting (telogen) hair follicles by wax depilation [26]. This was followed by topical tamoxifen application to the dorsal skin, to delete TAK1 (Fig. 4A). At 2 weeks after synchronized anagen induction, hair shaft formation was noted in the control mice, as a macroscopic indicator of well-advanced anagen development, while hair shaft growth was not seen in the tamoxifen-treated *Map3k7*$^{fl/fl}$K14-Cre-ER^{T2} mice (Fig. 4B). Histological analysis revealed that anagen progression was severely delayed in TAK1-deleted mice at 1–3 weeks (Fig. 4C).

Quantitative hair cycle histomorphometry and hair cycle score calculation (Fig. 5) confirmed that depilation-induced anagen progression was severely delayed in TAK1-deleted mice at 1–3 weeks, while anagen development progressed as expected in TAK1-competent mice. Taken together, these data suggest that

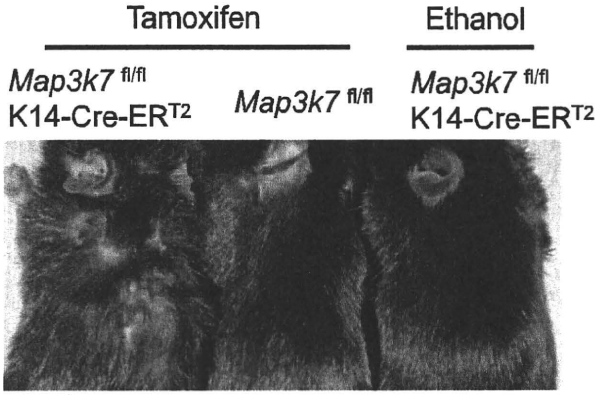

Figure 3. Keratinocyte-specific TAK1 deletion results in hair loss in adolescent mice. Tamoxifen was topically applied to the dorsal skin of the *Map3k7*$^{fl/fl}$K14-Cre-ER^{T2} mice for 5 consecutive days to delete TAK1. The clinical appearance of the mice 4 weeks after the application is shown. As controls, *Map3k7*$^{fl/fl}$ mice or *Map3k7*$^{fl/fl}$K14-Cre-ER^{T2} mice were treated with tamoxifen or ethanol, respectively.
doi:10.1371/journal.pone.0011275.g003

TAK1 is an important regulator of early anagen development in telogen hair follicles, although TAK1 does not appear to be indispensable for anagen induction.

Although leaky Cre- ER^{T2} activity was noted in ethanol-treated *Map3k7*$^{fl/fl}$K14-Cre-ER^{T2} mice (Fig. 2), there was no significant difference between ethanol-treated *Map3k7*$^{fl/fl}$K14-Cre-ER^{T2} mice and tamoxifen-treated *Map3k7*$^{fl/fl}$ mice. Therefore, leaky activity of Cre- ER^{T2} seems to have a minimum effect in this experiment.

Keratinocyte-specific TAK1 deletion causes a transition from anagen to dystrophic catagen in adolescent mice

In the third experimental setup, TAK1 was deleted only 1 week after anagen induction (Fig. 6A). At 2 weeks after depilation, hair regrowth was reduced in the tamoxifen-treated *Map3k7*$^{fl/fl}$K14-Cre-ER^{T2} mice (Fig. 6B), compared with controls. Histological analysis revealed that almost all of the hair follicles in tamoxifen-treated *Map3k7*$^{fl/fl}$K14-Cre-ER^{T2} mice had prematurely entered the apoptosis-driven regression stage of hair follicle cycle (i.e., catagen; Fig. 6C).

Interestingly, however, this accelerated catagen development was associated with striking pigmentary signs of hair follicle damage (dystrophy): many large, ectopically located melanin clumps, often larger than keratinocyte nuclei, were found not only in their normal location (i.e., the precortical hair matrix), but also eccentrically in the hair bulb periphery and in the epithelial strand of the involuting catagen hair follicles (Fig. 6D). Thus, TAK1 deletion induced "dystrophic catagen," an indicator of major hair follicle damage [28]. Quantitative analyses (Fig. 6E) confirmed that most of the hair follicles in tamoxifen-treated *Map3k7*$^{fl/fl}$K14-Cre-ER^{T2} mice were in late dystrophic catagen, while those of controls were in anagen. These data suggest that TAK1 is essential for maintaining a functional anagen phase.

Discussion

Here, we show by mouse genomics and targeted deletion experiments that TAK1, a member of the NF-κB pathway that has chiefly been recognized as a mediator of innate and adaptive immunity [1,2,4,5,6,30], is also a key component of the molecular machinery that controls murine hair growth. Consistent with our previous discovery that TAK1 regulates keratinocyte growth,

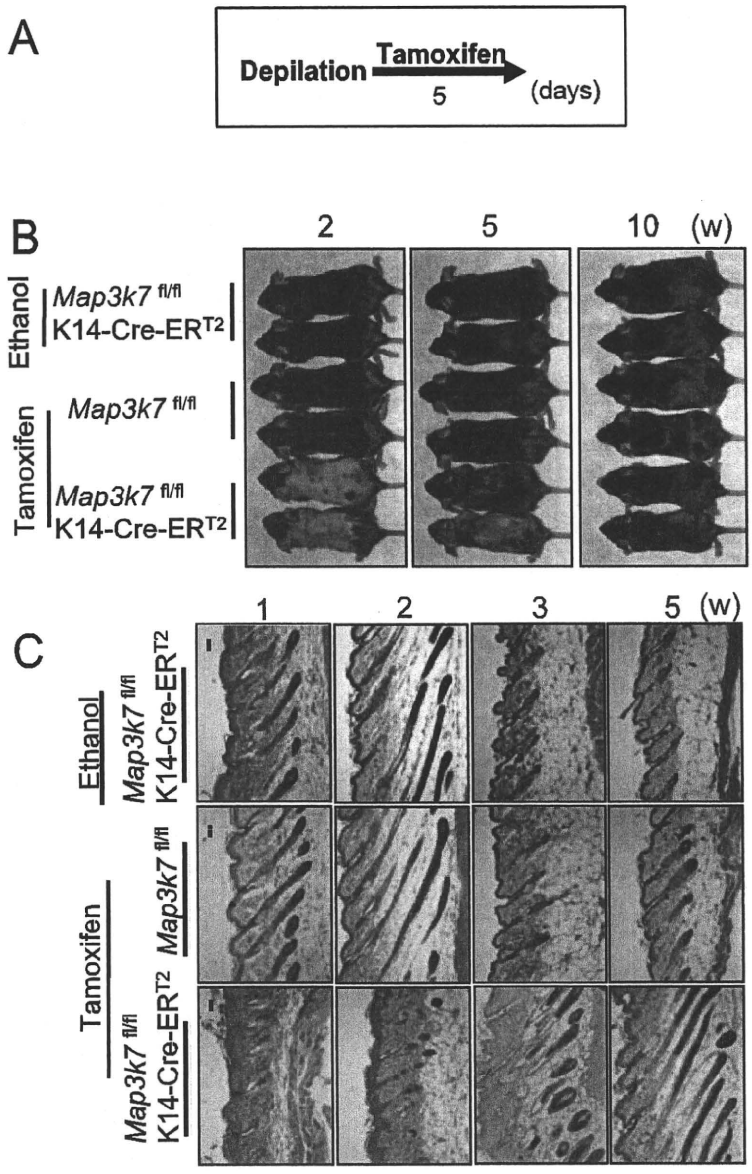

Figure 4. Keratinocyte-specific TAK1 deletion delays hair cycle progression in adolescent mice. (A) Schedule of tamoxifen application. The hair cycle was synchronized to anagen phase by wax depilation, and tamoxifen was topically applied to the dorsal skin of *Map3k7*$^{fl/fl}$K14-Cre-ER^{T2}mice to delete TAK1. As controls, *Map3k7*$^{fl/fl}$ mice or *Map3k7*$^{fl/fl}$K14-Cre-ER^{T2} mice were treated with tamoxifen or ethanol, respectively. (B) Clinical appearance at the indicated time point after the depilation. At 2 weeks, hair shaft formation was noted in the control mice, while hair shaft growth was not seen in the tamoxifen-treated *Map3k7*$^{fl/fl}$K14-Cre-ER^{T2} mice. (C) Histological analysis at the indicated time point after the depilation. Anagen progression was severely delayed in TAK1-deleted mice at 1–3 weeks. Scale bar, 100 μm.
doi:10.1371/journal.pone.0011275.g004

differentiation, and apoptosis [12], we now show that the selective deletion of TAK1 in keratinocytes retards hair follicle induction, morphogenesis, and anagen development, and is required for the maintenance of normal anagen. This newly identified role of TAK1 in hair follicle development and cycling implicates TAK1 as a novel player in complex organ remodeling events and epithelial-mesenchymal interactions, which can be modeled by murine hair follicles [11].

The TAK1-NF-κB pathway regulates not only immune responses [1,30], but also epithelial function [12]. Because the NF-κB pathway controls pro-inflammatory responses, deletion of this pathway was expected to suppress epithelial inflammation. Unexpectedly, however, deletion of TAK1, IKK-β, or IKK-γ was found to result in severe skin inflammation (including abscess formation) [12,31,32,33]. Similarly, a lack of NF-κB signaling produced by the conditional ablation of IKKγ or IKKα and IKKβ in the intestinal epithelium caused severe chronic intestinal inflammation in mice [34]. This suggests that a continuous, basal level of NF-κB activation may be required to maintain epithelial integrity and homeostasis and to suppress excessive skin inflammation. In the current study, we add to the established role of TAK1 in murine skin the novel function of hair growth control.

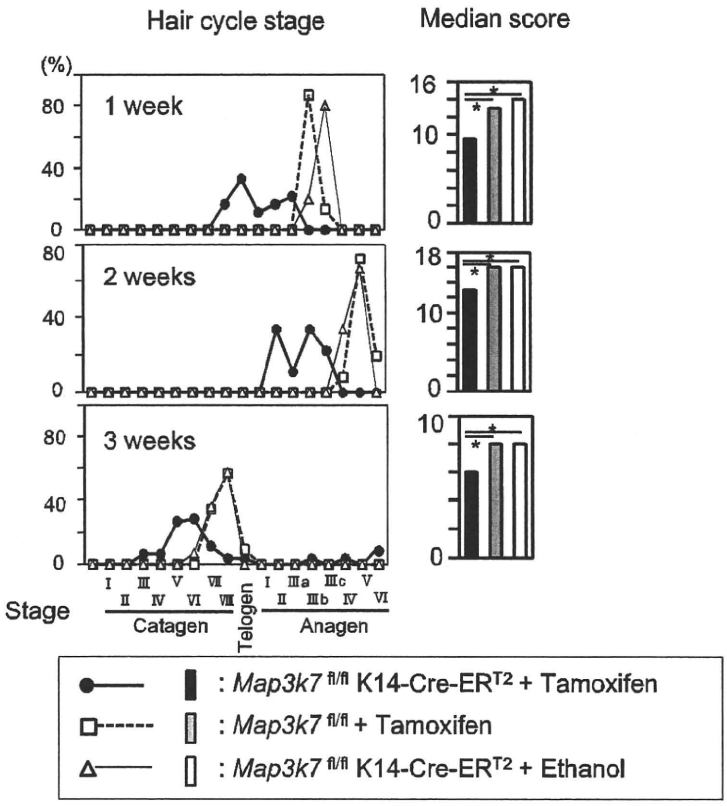

Figure 5. Quantitative hair cycle analysis. Hair cycle stage of each hair follicle in each mouse group in Fig. 4 was evaluated according to our previous report [27]. Then, the rate (%) of a certain hair cycle stage in the total hair follicles (left panel) and the median score in each mouse group (right panel) were determined. The score of tamoxifen-treated *Map3k7*$^{fl/fl}$K14-Cre-ER^{T2} mice was compared with tamoxifen-treated *Map3k7*$^{fl/fl}$ mice or ethanol-treated *Map3k7*$^{fl/fl}$K14-Cre-ER^{T2} mice. Statistical significance was determined using a Mann-Whitney's U-test. *$P<0.01$.
doi:10.1371/journal.pone.0011275.g005

Since TAK1 regulates keratinocyte function [12], there is a possibility that hair follicle defects in TAK1-deficient mice might be attributed to such abnormal capacities of keratinocytes rather than reflecting the specific function of TAK1 in hair follicle regulation. However, clinical skin pheno types and histological abnormalities were not apparent at birth and started to appear at P2 in *Map3k7*$^{fl/fl}$K5-Cre mice [12]. On the other hand, E15.5 is the time point when the defect of hair follicle development became apparent (Fig. 1). Therefore, the defect of hair follicle development is primarily due to the defect of TAK1 signaling during embryogenesis, rather than the functional defect of keratinocytes.

Recently, TAK1 binding protein (TAB) 2 has been identified as a binding partner of EdaR-associated death domain protein (EDARADD) using a yeast two-hybrid screening [35]. In 293 cells, endogenous and overexpressed TAB2, TRAF6 and TAK1 were co-immunoprecipitated with EDARADD [35]. Furthermore, dominant negative forms of TAB2, TRAF6 and TAK1 blocked the NF-κB activation induced by EDARADD in 293 cells[35]. Therefore, it is suggested that TAK1 is involved in hair follicle development. However, the actual role of TAK1 in hair follicle has not been studied before.

The coats of mice contain four major hair follicle subpopulations: guard hairs, awl and auchene hairs, and zigzag hairs. Formation of each kind of hair follicle starts at E14, E16, and E18-P3, respectively and the regulatory mechanisms of hair follicle development are slightly different among them [7,36]. Epidermal NF-κB activity is first observed in the placodes of primary guard hairs at E14.5 [36]. In the absence of NF-κB activity, downstream events, such as maintenance of Wnt signaling and an increase of Wnt10a, Wnt10b, and Dkk4 expression, are impaired [8] and further placode down-growth does not occur in primary guard hair follicles [36]. In *Map3k7*$^{fl/fl}$K5-Cre mice, the number of hair germs was significantly reduced at E15.5, indicating that the development of primary guard hair follicles was greatly impaired. Impaired development of primary guard hair follicles at E15.5 can be explained by the absence of NF-κB activity, due to TAK1 deficiency, consistent with a model in which TAK1 is involved in the EdaA1/EdaR/NF-κB pathway [35] (see Fig. 7). The appearance of a few primary hair placodes might be explained by incomplete TAK1 deletion at E15.5.

In contrast, EdaR/NF-κB activity is dispensable for the induction of awl/auchene hair follicles, as seen in *tabby*, *downless*, and $c^{I\kappa B\alpha\Delta N}$ mice, even though EdaR/NF-κB-defective, awl/auchene hair follicles subsequently produce abnormal awl-like hair shafts [36,37]. EdaR/NF-κB independent Wnt/β-catenin signaling is required for this process [8]. Thus, the placodes that became visible in *Map3k7*$^{fl/fl}$K5-Cre mice at E16.5 are likely to represent placodes of awl/auchene hair follicles. In a recent study, analyses of Eda and EdaR homologue Troy double-mutant mice revealed that, in addition to primary guard hair follicles, awl/auchene hair follicles were defective in these mice [38]. This study suggested that EdaR and Troy redundantly activate an NF-κB independent pathway, via TRAF6, to develop awl/auchene hair follicle placodes. Therefore, it is conceivable that placode development

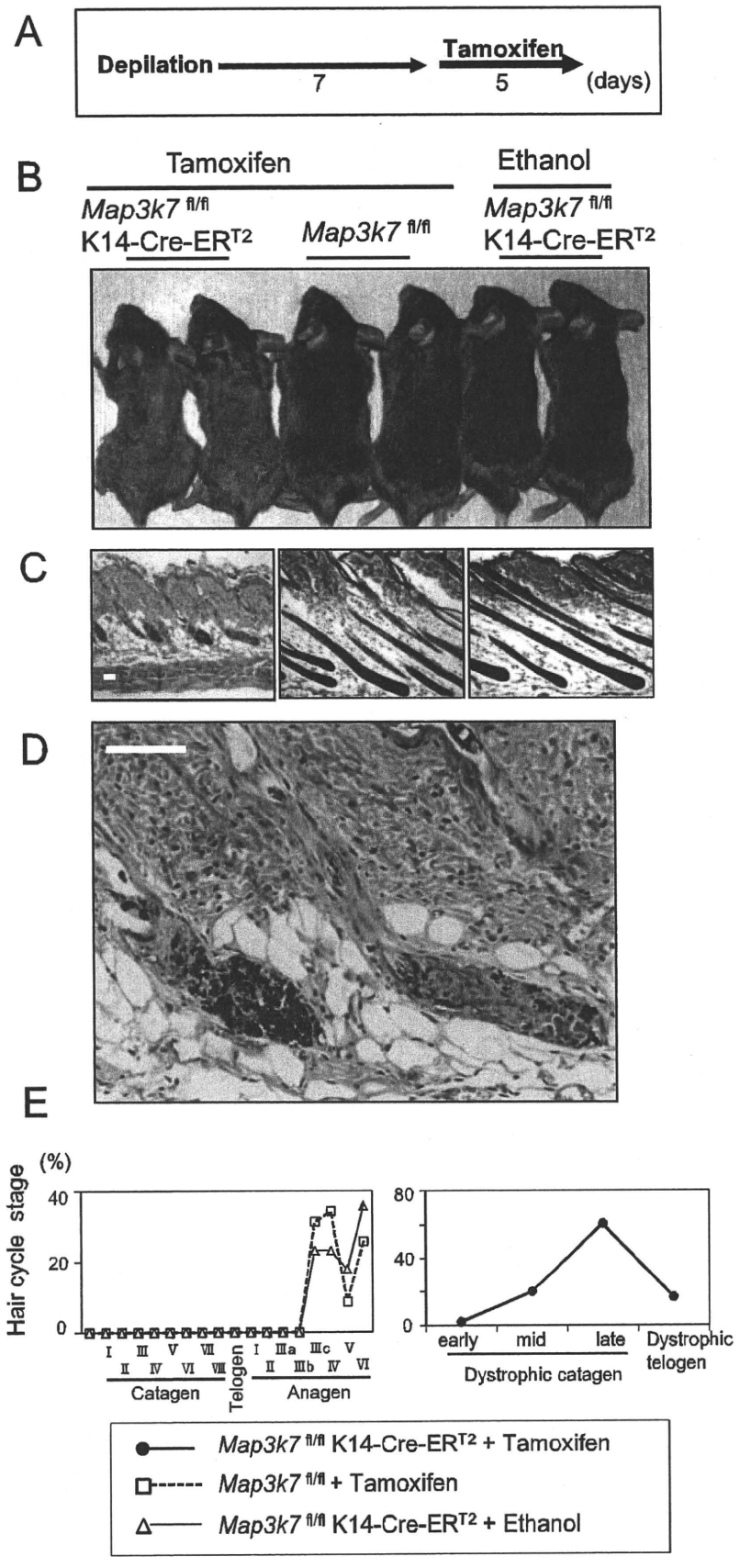
A
Depilation
7
Tamoxifen
5
(days)
B
Tamoxifen
Ethanol
Map3k7 fl/fl
K14-Cre-ERT2
Map3k7 fl/fl
Map3k7 fl/fl
K14-Cre-ERT2
C
D
E
Hair cycle stage
(%)
40
20
0
I III V VII
II IV VI VIII
Catagen
Telogen
I IIIa IIIc V
II IIIb IV VI
Anagen
80
40
0
early
mid
late
Dystrophic telogen
Dystrophic catagen
Map3k7 fl/fl K14-Cre-ERT2 + Tamoxifen
Map3k7 fl/fl + Tamoxifen
Map3k7 fl/fl K14-Cre-ERT2 + Ethanol

Figure 6. Keratinocyte-specific TAK1 deletion causes a transition from anagen to dystrophic catagen in adolescent mice. (A) Schedule of tamoxifen application. The hair cycle was synchronized to anagen phase by wax depilation. At 7 days after depilation, tamoxifen was applied for 5 days. (B) Clinical appearance of the mice 2 weeks after depilation. (C) Histological analysis of the mice 2 weeks after depilation. (D) Higher magnification of the tamoxifen-treated *Map3k7*$^{fl/fl}$K14-Cre-ER^{T2} mice in (C). Scale bar, 100 μm. (E) Dystrophic catagen was defined according to a previous report [28]. Then, the rate (%) of a certain hair follicle stage per total hair follicles was calculated. Quantitative analyses confirmed that most of the hair follicles in tamoxifen-treated *Map3k7*$^{fl/fl}$K14-Cre-ER^{T2} mice were in late dystrophic catagen, while those of controls were in anagen.
doi:10.1371/journal.pone.0011275.g006

in *Map3k7*$^{fl/fl}$K5-Cre mice is controlled by this NF-κB- (and TAK1)-independent pathway (Fig. 7).

Besides NF-κB signaling, recent studies indicate the implication of TAK1 in multiple signaling pathways such as MAP kinases and AP1 signaling [1,39], supporting the alternative possibility that, in addition to the NF-κB signaling pathway, multiple signaling pathways may be also involved in hair follicle regulation downstream to TAK1. Although some TNF receptor family activate JNK pathway in addition to NF-κB, Edar shows only weak activation of JNK/AP-1 pathway [14,20]. In contrast to Edar, Troy [40] leads to a strong activation of JNK pathway, but weak activation of NF-κB [20,40]. Therefore, it is possible Troy/TAK1/JNK/AP-1 pathway is involved in hair morphogenesis. However, this point should be further clarified.

An interesting difference was observed between *Map3k7*$^{fl/fl}$K5-Cre mice and *tabby*, *downless*, and $c^{IκBαΔN}$ mice. While *tabby*, *downless*, and $c^{IκBαΔN}$ mice produced abnormal awl-like hair shafts, *Map3k7*$^{fl/fl}$K5-Cre mice exhibited a prolonged morphogenesis period and did not develop hair shafts, even after skin transplantation onto normal control mice (unpublished, preliminary findings). This suggests that TAK1 deletion also affects the morphogenesis of the secondary hair follicles.

Although numerous molecular players have been identified as powerful regulators of hair follicle cycling, the exact molecular machinery that drives the elusive "hair cycle clock" remains unclear [29,41,42,43]. For example, IGF-1, HGF, glial-derived neurotrophic factor, and VEGF are known to prolong the duration of anagen, while fibroblast growth factor 5, TGFβ1 and TGFβ2, IL-1β, NT-3, estrogen receptor-mediated signaling, and IFN-γ are all known to induce the anagen-catagen transition [29,41,43,44,45]. The expression of regulatory molecules is controlled by upstream signals, such as those provided by the NF-κB, Wnt/β-catenin, bone morphogenetic protein (BMP), and Shh-Gli pathways [29,41,42]. On the basis of our findings, TAK1 should now be considered a part of the molecular machinery of the anagen induction.

In the present study, we have shown that TAK1 deletion severely delays the telogen-anagen transition, although it is not completely suppressed, while deletion of TAK1 in anagen follicles prematurely induces catagen and damages normal hair follicle function. Thus, TAK1 activity is important, but not essential, for anagen initiation and progression, yet is essential for the maintenance of mature anagen follicles, with loss of TAK1 activity resulting in catagen induction. The next challenge is to dissect the upstream and downstream signals of TAK1. Because NF-κB is thought to be a downstream signal of TAK1 in hair morphogenesis, and because strong NF-κB activity is detected in the anagen matrix of pelage follicles of adult mice [37], NF-κB is a major candidate downstream signal of TAK1 in anagen induction. Conversely, EdaR is a plausible candidate upstream signal of TAK1 because EdaA1 and EdaR have already been shown to be involved in hair follicle cycling [9,21,22].

After chemical, biological, or physical damage, hair follicles develop abnormalities that are collectively called hair follicle dystrophy [28]. Low follicular damage induces the "dystrophic anagen" response. Severe follicular damage induces the "dystrophic catagen" response, characterized by an immediate anagen termination. In Fig. 6, the hair follicle stage was defined as "dystrophic catagen". The development of "dystrophic catagen" indicates TAK1-deletion-induced follicular damage is comparatively higher and similar to those of high dose cyclophosphamide-induced alopecia. These suggest that TAK1-deletion-induced dystrophic catagen could be a model of chemotherapy-induced alopecia.

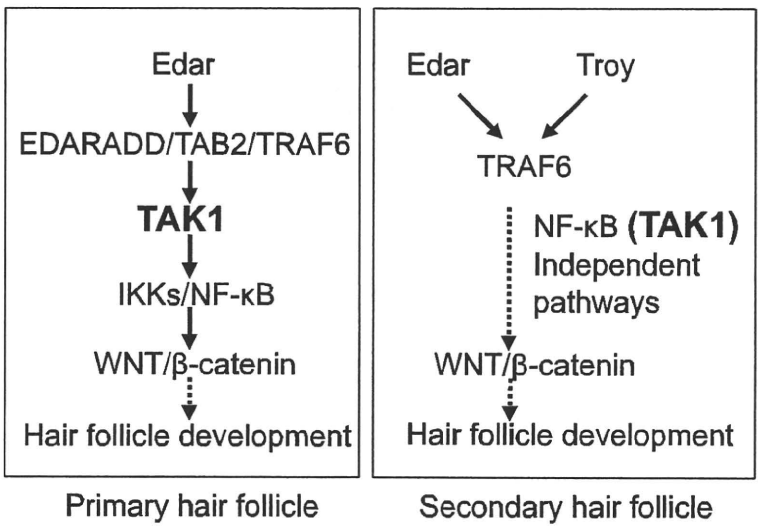

Figure 7. Model for the signaling pathways involved in hair follicle development. In the development of primary hair placodes, TAK1 is involved in the Edar/NF-κB pathway. In secondary hair placodes, NF-κB (TAK1)-independent pathways regulate hair placode development.
doi:10.1371/journal.pone.0011275.g007

The evidence reported here, that TAK1, a critical mediator of inflammation [1,30], is also involved in hair morphogenesis and anagen induction.

Acknowledgments

We thank Manabu Ohyama (Keio University, Tokyo, Japan), Teruko Tsuda, and Eriko Tan (Ehime University) for providing significant technical assistance.

References

1. Sato S, Sanjo H, Takeda K, Ninomiya-Tsuji J, Yamamoto M, et al. (2005) Essential function for the kinase TAK1 in innate and adaptive immune responses. Nat Immunol 6: 1087–1095.
2. Shim JH, Xiao C, Paschal AE, Bailey ST, Rao P, et al. (2005) TAK1, but not TAB1 or TAB2, plays an essential role in multiple signaling pathways in vivo. Genes Dev 19: 2668–2681.
3. Yamaguchi K, Shirakabe K, Shibuya H, Irie K, Oishi I, et al. (1995) Identification of a member of the MAPKKK family as a potential mediator of TGF-beta signal transduction. Science 270: 2008–2011.
4. Takaesu G, Kishida S, Hiyama A, Yamaguchi K, Shibuya H, et al. (2000) TAB2, a novel adaptor protein, mediates activation of TAK1 MAPKKK by linking TAK1 to TRAF6 in the IL-1 signal transduction pathway. Mol Cell 5: 649–658.
5. Takaesu G, Surabhi RM, Park KJ, Ninomiya-Tsuji J, Matsumoto K, et al. (2003) TAK1 is critical for IkappaB kinase-mediated activation of the NF-kappaB pathway. J Mol Biol 326: 105–115.
6. Ishitani T, Takaesu G, Ninomiya-Tsuji J, Shibuya H, Gaynor RB, et al. (2003) Role of the TAB2-related protein TAB3 in IL-1 and TNF signaling. Embo J 22: 6277–6288.
7. Schmidt-Ullrich R, Paus R (2005) Molecular principles of hair follicle induction and morphogenesis. Bioessays 27: 247–261.
8. Zhang Y, Tomann P, Andl T, Gallant NM, Huelsken J, et al. (2009) Reciprocal requirements for EDA/EDAR/NF-kappaB and Wnt/beta-catenin signaling pathways in hair follicle induction. Dev Cell 17: 49–61.
9. Tong X, Coulombe PA (2006) Keratin 17 modulates hair follicle cycling in a TNFalpha-dependent fashion. Genes Dev 20: 1353–1364.
10. Courtney JM, Blackburn J, Sharpe PT (2005) The Ectodysplasin and NFkappaB signalling pathways in odontogenesis. Arch Oral Biol 50: 159–163.
11. Schneider MR, Schmidt-Ullrich R, Paus R (2009) The hair follicle as a dynamic miniorgan. Curr Biol 19: R132–142.
12. Sayama K, Hanakawa Y, Nagai H, Shirakata Y, Dai X, et al. (2006) Transforming growth factor-beta-activated kinase 1 is essential for differentiation and the prevention of apoptosis in epidermis. J Biol Chem 281: 22013–22020.
13. Paus R, Muller-Rover S, Van Der Veen C, Maurer M, Eichmuller S, et al. (1999) A comprehensive guide for the recognition and classification of distinct stages of hair follicle morphogenesis. J Invest Dermatol 113: 523–532.
14. Mikkola ML, Thesleff I (2003) Ectodysplasin signaling in development. Cytokine Growth Factor Rev 14: 211–224.
15. Kere J, Srivastava AK, Montonen O, Zonana J, Thomas N, et al. (1996) X-linked anhidrotic (hypohidrotic) ectodermal dysplasia is caused by mutation in a novel transmembrane protein. Nat Genet 13: 409–416.
16. Ferguson BM, Brockdorff N, Formstone E, Ngyuen T, Kronmiller JE, et al. (1997) Cloning of Tabby, the murine homolog of the human EDA gene: evidence for a membrane-associated protein with a short collagenous domain. Hum Mol Genet 6: 1589–1594.
17. Srivastava AK, Pispa J, Hartung AJ, Du Y, Ezer S, et al. (1997) The Tabby phenotype is caused by mutation in a mouse homologue of the EDA gene that reveals novel mouse and human exons and encodes a protein (ectodysplasin-A) with collagenous domains. Proc Natl Acad Sci U S A 94: 13069–13074.
18. Yan M, Wang LC, Hymowitz SG, Schilbach S, Lee J, et al. (2000) Two-amino acid molecular switch in an epithelial morphogen that regulates binding to two distinct receptors. Science 290: 523–527.
19. Headon DJ, Emmal SA, Ferguson BM, Tucker AS, Justice MJ, et al. (2001) Gene defect in ectodermal dysplasia implicates a death domain adapter in development. Nature 414: 913–916.
20. Kumar A, Eby MT, Sinha S, Jasmin A, Chaudhary PM (2001) The ectodermal dysplasia receptor activates the nuclear factor-kappaB, JNK, and cell death pathways and binds to ectodysplasin A. J Biol Chem 276: 2668–2677.
21. Fessing MY, Sharova TY, Sharov AA, Atoyan R, Botchkarev VA (2006) Involvement of the Edar signaling in the control of hair follicle involution (catagen). Am J Pathol 169: 2075–2084.
22. Mustonen T, Pispa J, Mikkola ML, Pummila M, Kangas AT, et al. (2003) Stimulation of ectodermal organ development by Ectodysplasin-A1. Dev Biol 259: 123–136.
23. Tarutani M, Itami S, Okabe M, Ikawa M, Tezuka T, et al. (1997) Tissue-specific knockout of the mouse Pig-a gene reveals important roles for GPI-anchored proteins in skin development. Proc Natl Acad Sci U S A 94: 7400–7405.
24. Li M, Indra AK, Warot X, Brocard J, Messaddeq N, et al. (2000) Skin abnormalities generated by temporally controlled RXRalpha mutations in mouse epidermis. Nature 407: 633–636.
25. Indra AK, Warot X, Brocard J, Bornert JM, Xiao JH, et al. (1999) Temporally-controlled site-specific mutagenesis in the basal layer of the epidermis: comparison of the recombinase activity of the tamoxifen-inducible Cre-ER(T) and Cre-ER(T2) recombinases. Nucleic Acids Res 27: 4324–4327.
26. Paus R, Stenn KS, Link RE (1990) Telogen skin contains an inhibitor of hair growth. Br J Dermatol 122: 777–784.
27. Muller-Rover S, Handjiski B, van der Veen C, Eichmuller S, Foitzik K, et al. (2001) A comprehensive guide for the accurate classification of murine hair follicles in distinct hair cycle stages. J Invest Dermatol 117: 3–15.
28. Hendrix S, Handjiski B, Peters EM, Paus R (2005) A guide to assessing damage response pathways of the hair follicle: lessons from cyclophosphamide-induced alopecia in mice. J Invest Dermatol 125: 42–51.
29. Paus R, Foitzik K (2004) In search of the "hair cycle clock": a guided tour. Differentiation 72: 489–511.
30. Sato S, Sanjo H, Tsujimura T, Ninomiya-Tsuji J, Yamamoto M, et al. (2006) TAK1 is indispensable for development of T cells and prevention of colitis by the generation of regulatory T cells. Int Immunol 18: 1405–1411.
31. Stratis A, Pasparakis M, Markur D, Knaup R, Pofahl R, et al. (2006) Localized inflammatory skin disease following inducible ablation of I kappa B kinase 2 in murine epidermis. J Invest Dermatol 126: 614–620.
32. Makris C, Godfrey VL, Krahn-Senftleben G, Takahashi T, Roberts JL, et al. (2000) Female mice heterozygous for IKK gamma/NEMO deficiencies develop a dermatopathy similar to the human X-linked disorder incontinentia pigmenti. Mol Cell 5: 969–979.
33. Schmidt-Supprian M, Bloch W, Courtois G, Addicks K, Israel A, et al. (2000) NEMO/IKK gamma-deficient mice model incontinentia pigmenti. Mol Cell 5: 981–992.
34. Nenci A, Becker C, Wullaert A, Gareus R, van Loo G, et al. (2007) Epithelial NEMO links innate immunity to chronic intestinal inflammation. Nature 446: 557–561.
35. Morlon A, Munnich A, Smahi A (2005) TAB2, TRAF6 and TAK1 are involved in NF-kappaB activation induced by the TNF-receptor, Edar and its adaptator Edaradd. Hum Mol Genet 14: 3751–3757.
36. Schmidt-Ullrich R, Tobin DJ, Lenhard D, Schneider P, Paus R, et al. (2006) NF-kappaB transmits Eda A1/EdaR signalling to activate Shh and cyclin D1 expression, and controls post-initiation hair placode down growth. Development 133: 1045–1057.
37. Schmidt-Ullrich R, Aebischer T, Hulsken J, Birchmeier W, Klemm U, et al. (2001) Requirement of NF-kappaB/Rel for the development of hair follicles and other epidermal appendices. Development 128: 3843–3853.
38. Pispa J, Pummila M, Barker PA, Thesleff I, Mikkola ML (2008) Edar and Troy signalling pathways act redundantly to regulate initiation of hair follicle development. Hum Mol Genet 17: 3380–3391.
39. Sakurai H, Nishi A, Sato N, Mizukami J, Miyoshi H, et al. (2002) TAK1-TAB1 fusion protein: a novel constitutively active mitogen-activated protein kinase kinase kinase that stimulates AP-1 and NF-kappaB signaling pathways. Biochem Biophys Res Commun 297: 1277–1281.
40. Kojima T, Morikawa Y, Copeland NG, Gilbert DJ, Jenkins NA, et al. (2000) TROY, a newly identified member of the tumor necrosis factor receptor superfamily, exhibits a homology with Edar and is expressed in embryonic skin and hair follicles. J Biol Chem 275: 20742–20747.
41. Stenn KS, Paus R (2001) Controls of hair follicle cycling. Physiol Rev 81: 449–494.
42. Alonso L, Fuchs E (2006) The hair cycle. J Cell Sci 119: 391–393.
43. Ohnemus U, Uenalan M, Inzunza J, Gustafsson JA, Paus R (2006) The hair follicle as an estrogen target and source. Endocr Rev 27: 677–706.
44. Mecklenburg L, Tobin DJ, Muller-Rover S, Handjiski B, Wendt G, et al. (2000) Active hair growth (anagen) is associated with angiogenesis. J Invest Dermatol 114: 909–916.
45. Lindner G, Menrad A, Gherardi E, Merlino G, Welker P, et al. (2000) Involvement of hepatocyte growth factor/scatter factor and met receptor signaling in hair follicle morphogenesis and cycling. Faseb J 14: 319–332.

Author Contributions

Conceived and designed the experiments: KS KH. Performed the experiments: KS KK KS SS YH XD. Analyzed the data: KS SH YS YIT RP JK. Contributed reagents/materials/analysis tools: DM PC SA. Wrote the paper: KS RP.

THE JOURNAL OF BIOLOGICAL CHEMISTRY VOL. 285, NO. 39, pp. 30042–30049, September 24, 2010

E2 Polyubiquitin-conjugating Enzyme Ubc13 in Keratinocytes Is Essential for Epidermal Integrity*

Received for publication, January 21, 2010, and in revised form, July 5, 2010 Published, JBC Papers in Press, July 27, 2010, DOI 10.1074/jbc.M110.106484

Koji Sayama[‡1,2], Masahiro Yamamoto[§1], Yuji Shirakata[‡], Yasushi Hanakawa[‡], Satoshi Hirakawa[‡], Xiuju Dai[‡], Mikiko Tohyama[‡], Sho Tokumaru[‡], Myoung-Sook Shin[¶], Hiroaki Sakurai[¶], Shizuo Akira[§], and Koji Hashimoto[‡]

From the [‡]Department of Dermatology, Ehime University Graduate School of Medicine, Ehime 791-0295, Japan, the [§]Research Institute for Microbial Disease, Osaka University, Suita 565-0871, Japan, and the [¶]Division of Pathogenic Biochemistry, Institute of Natural Medicine, University of Toyama, Toyama 930-0194, Japan

The E2 polyubiquitin-conjugating enzyme Ubc13 is a mediator of innate immune reactions. Ubc13 mediates the conjugation of keratin (K)63-linked polyubiquitin chains onto TNF receptor-associated factor 6 and IKKγ during NF-κB activation. In contrast to K48-linked polyubiquitin chains, K63-linked polyubiquitin chains function in nonproteasomal biological processes. Although Ubc13 has been shown to be critical for Toll-like receptor (TLR) and IL-1 receptor signaling, the function of Ubc13 in the epidermis has not been studied. We generated keratinocyte-specific Ubc13-deficient mice (*Ubc13*$^{flox/flox}$K5-Cre). At birth, the skin of the *Ubc13*$^{flox/flox}$K5-Cre mice was abnormally shiny and smooth; in addition, the mice did not grow and died by postnatal day 2. Histological analysis showed atrophy of the epidermis with keratinocyte apoptosis. Immunohistochemical analyses revealed reduced proliferation, abnormal differentiation, and apoptosis of keratinocytes in the *Ubc13*$^{flox/flox}$K5-Cre mouse epidermis. In culture, *Ubc13*$^{flox/flox}$K5-Cre keratinocyte growth was impaired, and spontaneous cell death occurred. Moreover, the deletion of Ubc13 from cultured *Ubc13*$^{flox/flox}$ keratinocytes by means of an adenoviral vector carrying Cre recombinase also resulted in spontaneous cell death. Therefore, Ubc13 is essential for keratinocyte growth, differentiation, and survival. Analyses of intracellular signaling revealed that the IL-1 and TNF-induced activation of JNK, p38, and NF-κB pathways was impaired in *Ubc13*$^{flox/flox}$K5-Cre keratinocytes. In conclusion, Ubc13 appears to be essential for epidermal integrity in mice.

The NF-κB, JNK, and p38 intracellular signaling cascades mediate innate immune or pro-inflammatory responses such as TLR, IL-1 receptor, and TNF receptor signaling (1, 2). Upon stimulation, TNF receptor-associated factor 6 is polyubiquitinated, which induces it to phosphorylate TGF-β-activated kinase 1 (TAK1)[3] (3, 4). The polyubiquitin chains on TNF receptor-associated factor 6 are generated by the E2 ubiquitin-conjugating enzyme Ubc13 (3, 5). Ubc13 conjugates keratin (K)63-linked polyubiquitin chains to TNF receptor-associated factor 6 and IKK-γ. In contrast to K48-linked polyubiquitin chains, K63-linked polyubiquitin chains function in nonproteasomal biological processes, such as stress responses, rather than protein destruction. However, the role of these signaling molecules varies by cell type and stimulus.

Epidermal keratinocytes proliferate at the basal cell layer and then differentiate to form the multilayered epidermis, which serves as a physical barrier against the external environment. The proliferation and differentiation of keratinocytes are regulated by intracellular signaling pathways, including those mediated by NF-κB, MAPK, and PI3K (6–8). In this study, we focused on the NF-κB pathway. Genetic studies have shown that mutations in *NEMO/IKK-γ* cause incontinentia pigmenti or Bloch-Sulzberger syndrome in humans (9). The disruption of *NEMO/IKK-γ* leads to hyperproliferation and increased apoptosis in keratinocytes (10, 11). The functional blockade of NF-κB *in vivo* by the expression of a dominant-negative mutant of NF-κB in mouse epidermis resulted in a hyperplastic epithelium (6). Similarly, a deficiency in the p65 subunit of NF-κB caused hyperplasia of the epidermis (12). In addition to the regulation of differentiation and cell growth, NF-κB protects keratinocytes from apoptosis. The blockade of NF-κB function in the epidermis by the expression of a dominant-negative mutant of IκBα provoked premature spontaneous cell death (13). TAK1 is a critical mediator of NF-κB activation. Previously, we generated keratinocyte-specific TAK1-deficient mice and showed that along with IKKs, TAK1 regulates keratinocyte growth, differentiation, and apoptosis (14).

Because Ubc13 functions in the NF-κB signaling pathway, it might be expected to regulate keratinocyte growth, differentiation, and apoptosis. However, the function of Ubc13 in epidermal keratinocytes has not been studied. To address this issue, we generated keratinocyte-specific Ubc13-deficient mice by breeding *Ubc13*$^{flox/flox}$ mice (15) with mice carrying the Cre transgene under the control of the keratin-5 promoter (K5-Cre) (16).

* This work was supported by grants from the Ministries of Education, Culture, Sports, Science, and Technology of Japan; by Health and Labor Sciences Research Grants (Research on Intractable Diseases) from the Ministry of Health, Labor, and Welfare of Japan; and by grants from the Takeda Science Foundation, Mishima Kaiun Memorial Foundation, Mochida Memorial Foundation for Medical and Pharmaceutical Research, Naito Foundation, Kowa Life Science Foundation, and the Yasuda Medical Foundation.

[1] Both authors contributed equally to this work.

[2] To whom correspondence should be addressed: Dept. of Dermatology, Ehime University Graduate School of Medicine, Toon, Ehime 791-0295, Japan. Fax: 81-89-960-5352; E-mail: sayama@m.ehime-u.ac.jp.

[3] The abbreviations used are: TAK1, TGF-β-activated kinase 1; K, keratin; Ax, adenoviral vector; LDH, lactate dehydrogenase; HB-EGF, heparin-binding EGF-like growth factor; TLR, toll-like receptor; TRAIL, TNF-related apoptosis-inducing ligand.

EXPERIMENTAL PROCEDURES

Generation of Keratinocyte-specific Ubc13-deficient Mice Using Gene Targeting with the Cre Transgene—The targeting construct was described previously (15). *Ubc13*$^{flox/flox}$ mice were bred with K5-Cre mice (generous gift from Junji Takeda, Osaka University, Osaka, Japan) (16) to generate K5-Cre/*Ubc13*$^{flox/+}$ mice. Subsequently, the K5-Cre/*Ubc13*$^{flox/+}$ mice were bred with *Ubc13*$^{flox/flox}$ mice to generate K5-Cre/*Ubc13*$^{flox/flox}$ mice. This protocol was approved by the Institutional Review Board of the Ehime University Graduate School of Medicine.

The genotype was confirmed by Southern and Western blotting as described previously (15). Genomic DNA was extracted from the tails of the mice, digested with NcoI and ScaI, electrophoresed, and hybridized with a radiolabeled probe (15). For Western blot analysis, newborn mouse keratinocytes were cultured overnight, and adherent keratinocytes were harvested for analysis.

Histological Analysis—To analyze the expression of the differentiation markers K5, K14, K1, K10, and loricrin, paraffin-embedded sections were deparaffinized, blocked with 10% goat serum, and reacted with primary antibodies overnight at 4 °C. After washing, the antibodies were detected using a peroxidase staining kit (ImmPRESS; Vector Laboratories, Burlingame, CA) and visualized with aminoethyl carbazole. For K15 and Ki67 staining, the deparaffinized sections were boiled in 10 mM citrate buffer, pH 6.0, for 40 min and cooled at room temperature for 20 min for antigen retrieval.

TUNEL—Keratinocyte apoptosis was detected using the TUNEL method as described previously (14) using an *in situ* detection kit (Roche Applied Science).

Antibodies—The following antibodies were used: Covance); Ki67 (MM1; Novo Castra); β-actin (AC-15; Abcam); IKK-γ (sc-8330; Santa Cruz Biotechnology); ubiquitin (P4D1; Santa Cruz Biotechnology); mouse TNF-α (goat; R & D Systems); and Ubc13 (4E11; Zymed Laboratories); cIAP-2 (mouse; R & D Systems); and caspase-3 (rabbit; Cell Signaling Technology). Antibodies specific for the phosphorylation forms of ERK (9101), JNK (9251), and p38 (9211) were purchased from Cell Signaling Technology.

Preparation of the Ax—An Ax encoding Cre-recombinase (Ax-Cre) was prepared as described previously (14). We infected the keratinocytes with the Ax at a multiplicity of infection of 100. Ax carrying LacZ (Ax-LacZ) was used as a control.

Keratinocyte Culture—Primary mouse keratinocytes were isolated from newborn mouse skin and cultured as described previously (14) using CnT-07 medium (CellnTec, Bern, Switzerland).

For the analysis of cell growth, freshly isolated newborn mouse keratinocytes were allowed to adhere to the culture dishes for several hours, and the nonadherent cells were removed by washing. The number of adherent cells was counted using a Coulter Counter (Beckman Coulter); this was denoted day 0. Cell culture continued for 3 days. The number of cells at day 0 was referred to as 100%.

For cytotoxic analysis, freshly isolated newborn mouse keratinocytes were stimulated with mouse TNF-α (Kamiya Biomedical Company; 10 ng/ml) or anti-mouse TNF-α (5 μg/ml). At 48 h, the supernatant was harvested for use in the LDH assay. Next, Ubc13 was deleted in *Ubc13*$^{flox/flox}$ keratinocytes by transfection of Ax-Cre at a multiplicity of infection of 100. Finally, 24 h after transfection, keratinocytes were stimulated with TNF-α or anti-TNF-α for 48 h. For analysis of intracellular signaling, freshly isolated newborn mouse keratinocytes were stimulated soon after adherence to cell culture dishes with IL-1β (PeproTech EC, London, UK; 10 ng/ml), TNF-α (10 ng/ml), or HB-EGF (R & D Systems; 10 ng/ml).

Western Blotting—Keratinocytes were harvested on ice with lysis buffer, and Western blotting was performed as described previously (8) using a FluoroImager (Molecular Dynamics). Phosphorylation of TAK1 was analyzed as described previously (1).

Immunoprecipitation—The cell lysates were precleaned with protein G-Sepharose (Amersham Biosciences) for 2 h and then incubated with protein G-Sepharose containing 1.0 μg of anti-IKK-γ for 12 h with rotating at 4 °C. After washing, the sample was eluted by boiling with sample buffer and then subjected to Western blot analysis using anti-ubiquitin as described previously (15).

LDH Assay—Cell death was quantitated by measuring LDH release using an LDH assay kit (Kyokutokogyo, Tokyo, Japan) according to the manufacturer's instructions. LDH from the living cells was obtained by cell lysis with 0.1% Tween 20. LDH release was expressed as a percentage of the total LDH, which was obtained by summing the LDH released and the LDH of the living cells. The data are expressed as the means ± S.E.

EMSA—Nuclear proteins were isolated, and 5 μg of proteins were applied for EMSA analyses as described previously (17) using a Light Shift Chemiluminescent EMSA kit (Pierce) according to the manufacturer's instructions. Specific NF-κB probe sets (biotin-labeled and unlabeled probes) were obtained from Panomics (Redwood City, CA). Protein-DNA complexes were separated and transferred to Biodyne B nylon membranes (Pierce). In competition experiments, unlabeled probes were added at 200-fold molar excess. The biotin-labeled molecules in the membranes were detected using a Chemiluminescent nucleic acid detection module (Pierce) and exposed to x-ray film.

Real Time PCR—Newborn mouse epidermis was separated from the dermis by heat treatment at 60 °C for 30 s. mRNA was extracted from the epidermis and was subjected to real time PCR analyses as described previously (18). The primers and the probes used for GAPDH, IL-1β, and TNF-α were obtained from Applied Biosystems (Branchburg, NJ). Gene expression levels were quantified using the comparative CT method and were normalized against GAPDH (18). The mean value of *Ubc13*$^{flox/flox}$ mice was referred to as 1.0 unit.

Luciferase Assay—pNFκB-TA-Luc (Clontech) was transfected to the keratinocytes. To normalize the transfection efficiency, pRL-TK (Promega) was included in the assay. The reporter plasmids were introduced into keratinocytes using FuGENE 6 (Roche Applied Science) according to the manufacturer's instructions. After treatment, the same number of cells was harvested with 250 μl of lysis buffer (Promega), and the luciferase activity was measured using the dual luciferase reporter

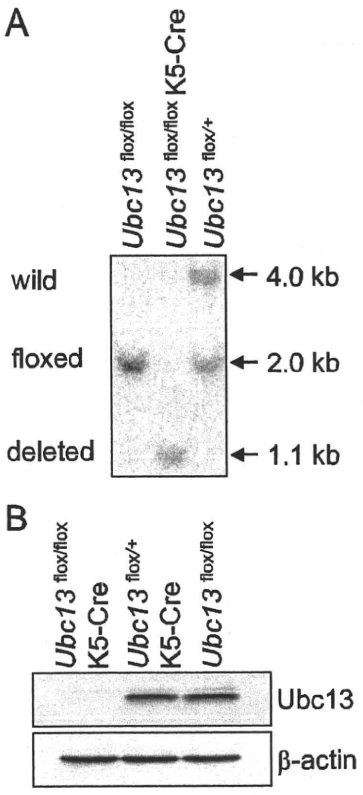

FIGURE 1. **Generation of keratinocyte-specific Ubc13-deficient mice.** Keratinocyte-specific Ubc13-deficient mice were generated by breeding $Ubc13^{flox/flox}$ mice (15) with K5-Cre mice (16). Southern (*A*) and Western (*B*) blotting confirmed the genotype. *A*, genomic DNA was extracted from mouse tails, digested with NcoI and ScaI, electrophoresed, and hybridized with a radiolabeled probe (15). *4.0-kb band*, wild-type allele; *2.0-kb band*, floxed allele; *1.1-kb band*, deleted allele. *B*, newborn mouse keratinocytes were cultured overnight, and the adherent keratinocytes were harvested for Western blot analysis. β-Actin was used as an internal standard.

assay system (Promega) with a luminometer (Luminescencer JNR AB-2100; Atto, Japan). The relative luciferase activity was calculated by normalizing to the level of *Renilla* luciferase activity.

Statistical Analysis—Statistical significance was determined using a paired Student's *t* test. A difference of $p < 0.01$ (*) or $p < 0.05$ (**) was considered statistically significant.

RESULTS

Generation of Keratinocyte-specific Ubc13-deficient Mice—Because the germ line deletion of *Ubc13* results in embryonic lethality (15), we generated keratinocyte-specific Ubc13-deficient mice by breeding $Ubc13^{flox/flox}$ mice (15) with K5-Cre mice (16). Southern and Western blot analyses showed the efficient deletion of Ubc13 in keratinocytes collected from $Ubc13^{flox/flox}$ K5-Cre mice at birth (Fig. 1).

Skin Phenotypes of the $Ubc13^{flox/flox}$K5-Cre Mice at Birth—At birth, the skin of the $Ubc13^{flox/flox}$ K5-Cre mice was abnormally shiny and smooth (Fig. 2*A*). In addition, the mice did not grow and died by postnatal day 2. In comparison, $Ubc13^{flox/+}$ and $Ubc13^{+/+}$ mice with or without K5-Cre showed no pathological phenotypes.

Histological analysis revealed atrophy of the epidermis in the $Ubc13^{flox/flox}$ K5-Cre mice (Fig. 2*B*), indicating that cell growth is impaired by the deletion of Ubc13. Ki67 staining showed decreased keratinocyte proliferation, whereas H&E staining and TUNEL revealed the presence of a small number of apoptotic cells, in the epidermis of each $Ubc13^{flox/flox}$ K5-Cre mouse (Fig. 2*B*). Ki67-positive cells/basal cells were 90.5 and 40% ($p < 0.01$, $n = 4$) in $Ubc13^{flox/flox}$ mice and $Ubc13^{flox/flox}$ K5-Cre mice, respectively. Apoptotic cells/basal cells were 0 and 2.9% ($p < 0.01$, $n = 4$) in $Ubc13^{flox/flox}$ mice and $Ubc13^{flox/flox}$ K5-Cre mice, respectively. Taken together, these results indicate that Ubc13 regulates keratinocyte growth and apoptosis in mice.

Because disruption of the NF-κB pathway causes inflammation in the skin (10, 11, 14, 19), the expression of pro-inflammatory cytokines in the epidermis was studied. Real time PCR analysis revealed that TNF-α mRNA expression was decreased, whereas IL-1α expression was increased in $Ubc13^{flox/flox}$K5-Cre mouse epidermis (Fig. 2*C*).

Abnormal Keratinocyte Differentiation in $Ubc13^{flox/flox}$K5-Cre Mouse Epidermis—To analyze the differentiation status of the epidermal keratinocytes, we performed immunohistochemical analyses using skin sections treated with antibodies specific for various differentiation markers (Fig. 3). According to our data, the suprabasal keratinocytes in the epidermis of the $Ubc13^{flox/flox}$ K5-Cre mice expressed K14, which is normally confined to the basal layer. Loricrin is a marker of late phase keratinocyte differentiation and is normally expressed in the upper epidermis, as shown in the control mice. Loricrin expression was absent from the viable epidermal keratinocytes of the $Ubc13^{flox/flox}$ K5-Cre mice. K15 is a marker of the bulge area in adult mice and is also expressed at the basal cell layer in neonatal mice (20), as shown in Fig. 2. However, K15 expression was absent from the epidermis of the $Ubc13^{flox/flox}$ K5-Cre mice. These results indicate that keratinocyte differentiation is disrupted by the deletion of Ubc13 in keratinocytes.

Impaired Cell Growth and Spontaneous Cell Death by Ubc13 Deletion—Keratinocytes were isolated from newborn mouse epidermis and cultured for cellular function analyses. Ubc13-deficient keratinocytes had growth impairments as shown in Fig. 4*A*. Furthermore, spontaneous cell death occurred, and the dead cells were positive for TUNEL (Fig. 4*B*). Analysis of LDH release revealed that cell death began within 1 day of adherence to the culture dishes and increased over 3 days (Fig. 4*C*). Because blockade of NF-κB pathway in keratinocytes enhances susceptibility to apoptosis by TNF-α (21), the cells were treated with TNF-α. The spontaneous cell death was slightly enhanced by TNF-α but was not blocked by anti-TNF-α antibodies (Fig. 4*D*).

Next, Ubc13 was deleted in cultured keratinocytes derived from $Ubc13^{flox/flox}$ mice, and Ax-Cre was transfected into cultured keratinocytes from $Ubc13^{flox/flox}$ or $Ubc13^{+/+}$ mice using Ax-LacZ as a control. Ubc13 expression began to decrease at 36 h after transfection with Ax-Cre (Fig. 5*A*). The deletion of Ubc13 in the cultured keratinocytes resulted in cell death, and the dead cells were positive for TUNEL (Fig. 5*B*). Similar to Fig. 4*D*, cell death was slightly enhanced by TNF-α but was not blocked by anti-TNF-α antibodies (Fig. 5*D*). These data indicate that Ubc13 is essential for keratinocyte survival. To further

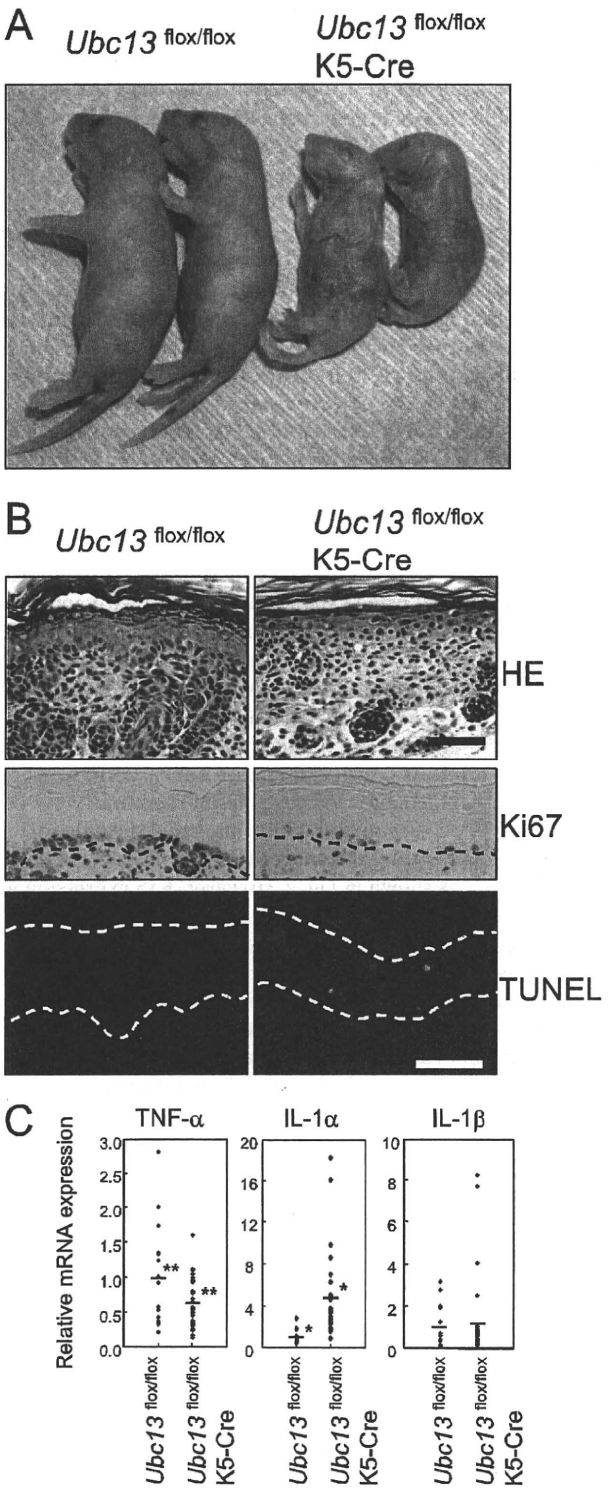

FIGURE 2. **Skin phenotypes of the *Ubc13*$^{flox/flox}$ K5-Cre mice.** *A*, appearance of the *Ubc13*$^{flox/flox}$ K5-Cre mice at postnatal day 1. The skin of the mice was abnormally shiny and smooth. *B*, histological analysis of *Ubc13*$^{flox/flox}$ K5-Cre mouse skin sections by H&E staining, Ki67 staining, and TUNEL. H&E staining showed atrophy of the epidermis in the *Ubc13*$^{flox/flox}$ K5-Cre mice. Ki67 staining showed decreased numbers of positive cells in the epidermis of the *Ubc13*$^{flox/flox}$K5-Cre mice. The epidermis also contained a few apoptotic cells as shown by H&E staining and TUNEL. The *dotted lines* indicate the basement membrane in the Ki67 section and the basement membrane and surface of the epidermis in the TUNEL section. *Ubc13*$^{flox/flox}$ represents the undeleted controls. *Scale bar*, 100 μm. *C*, mRNA expression of TNF-α, IL-1α, and IL-1β in the epidermis. Newborn mouse epidermis was separated from the dermis, and mRNA expression was analyzed by real time PCR. mRNA expression levels were normalized against GAPDH, and the mean value of *Ubc13*$^{flox/flox}$ mice was referred to as 1.0 unit. $n = 17$ (*Ubc13*$^{flox/flox}$ mice). $n = 28$ (*Ubc13*$^{flox/flox}$ K5-Cre mice). *, $p < 0.01$. **, $p < 0.05$.

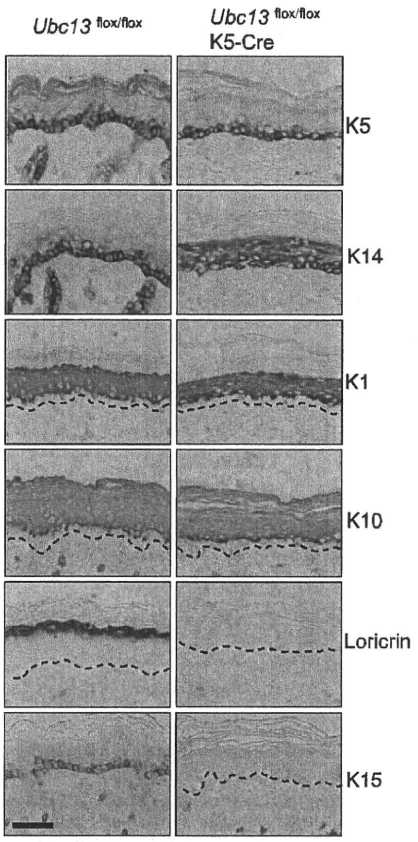

FIGURE 3. **Abnormal expression of differentiation markers in the epidermis of *Ubc13*$^{flox/flox}$K5-Cre mice.** The expression of various differentiation markers in the epidermis was analyzed immunohistochemically. The expression of K5 and K14 is normally confined to the basal cell layer. The expression of K1, K10, and loricrin marks suprabasal and late phase differentiation, whereas K15 is expressed at the basal cell layer in neonatal mouse epidermis. The *dotted lines* indicate the basement membrane. *Ubc13*$^{flox/flox}$ represents the undeleted controls. *Scale bar*, 100 μm.

study the mechanisms of spontaneous cell death, the expression of anti-apoptotic protein cIAP-2 and the activation of caspase-3 (22) were analyzed by Western blot (Fig. 5*E*). The expression of cIAP-2 was reduced by Ubc13 deletion, which was correlated with the activation of caspase-3.

Impaired Activation of p38, JNK, and NF-κB in Ubc13-deficient Keratinocytes—To study the cause of these functional defects of Ubc13-deficient keratinocytes, intracellular signals were analyzed. Because spontaneous cell death occurs, freshly isolated keratinocytes were stimulated soon after adherence to the culture dishes (Fig. 6). Neither p38 nor JNK was phosphorylated in the Ubc13-deficient keratinocytes by IL-1β or TNF-α, although both were phosphorylated within 15 min in the control keratinocytes (Fig.

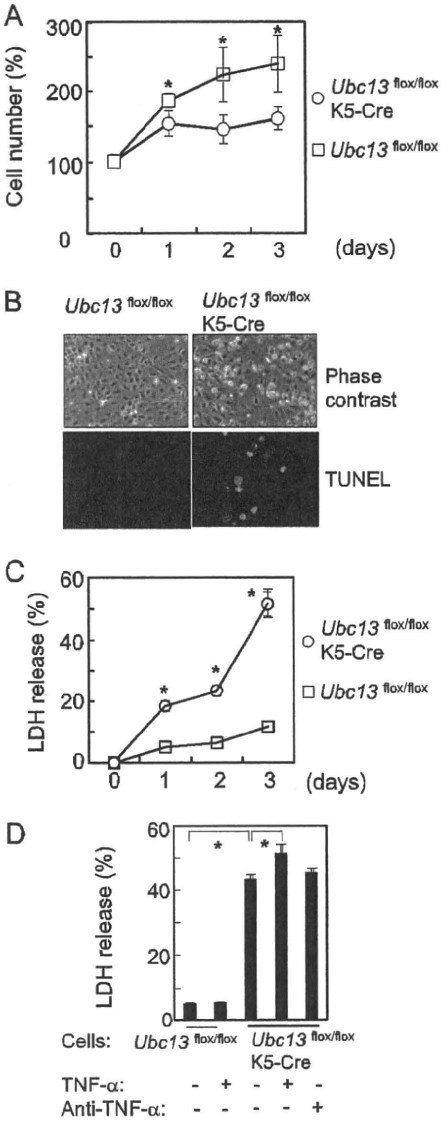

FIGURE 4. **Impaired cell growth and spontaneous cell death of *Ubc13*$^{flox/flox}$K5-Cre keratinocytes.** *A*, cell growth analysis. Freshly isolated newborn mouse keratinocytes were cultured for 3 days, and the number of cells was counted each day using a Coulter counter ($n = 6$). The number of cells at day 0 was referred to as 100%. *B*, cell morphology was examined by phase contrast microscopy, and apoptotic cells were detected using TUNEL after 2 days of culturing. *C*, cell death was quantified by measuring LDH release ($n = 6$). *D*, cytotoxic effects of TNF-α. Freshly isolated mouse keratinocytes were stimulated with mouse TNF-α (10 ng/ml) or goat anti-mouse TNF-α antibody (5 μg/ml). After 48 h, the supernatant was harvested for LDH assay. The data are expressed as the means ± S.E. ($n = 6$). *, $p < 0.01$.

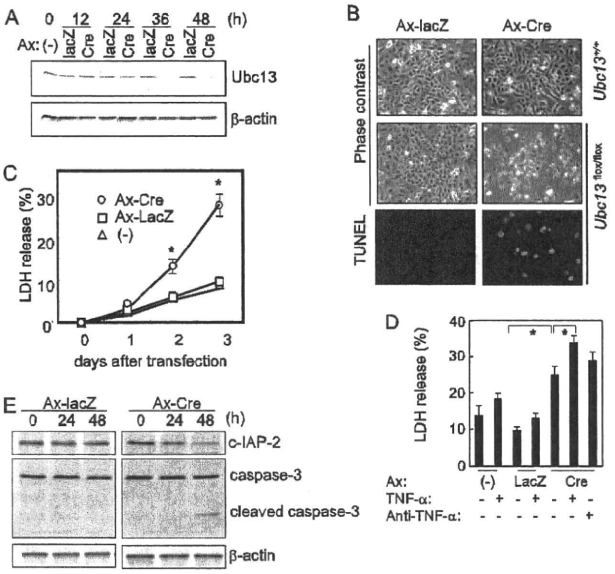

FIGURE 5. **Spontaneous cell death by deletion of Ubc13 using Ax-Cre.** Ubc13 was deleted from cultured keratinocytes derived from *Ubc13*$^{flox/flox}$ mice. Ax-Cre was transfected into the cultured keratinocytes of *Ubc13*$^{flox/flox}$ mice or *Ubc13*$^{+/+}$ mice at an multiplicity of infection of 100. Ax-LacZ was used as a control. *A*, the expression of Ubc13 in keratinocytes was analyzed by Western blotting using β-actin as an internal standard. *B*, cell morphology was examined by phase contrast microscopy, whereas apoptotic cells were detected using TUNEL at 72 h post-transfection. *C*, cell death was quantified by measuring LDH release. Ax was transfected into the cultured keratinocytes, and the culture supernatant was harvested for LDH assay at the indicated time ($n = 5$). *D*, cytotoxic effects of TNF-α. Freshly isolated *Ubc13*$^{flox/flox}$ keratinocytes were transfected with Ax at a multiplicity of infection of 100. After 24 h, the cells were stimulated with mouse TNF-α (10 ng/ml) or goat anti-mouse TNF-α antibody (5 μg/ml). After 48 h, the supernatant was harvested for use in the LDH assay ($n = 6$). The data are expressed as the means ± S.E. *, $p < 0.01$. *E*, the expression of c-IAP-2 and caspase-3 were analyzed by Western blot using β-actin as an internal standard.

6*A*). Activation of NF-κB pathway by IL-1β or TNF-α was also impaired in Ubc13-deficient keratinocytes as shown by Western blotting of IκB (Fig. 6*B*) and EMSA (Fig. 6*C*). Next, to study whether TAK1 is involved in this impaired NF-κB activation, the phosphorylation of TAK1 was analyzed. Although TAK1 was phosphorylated by IL-1β or TNF-α within 10 min in control keratinocytes, TAK1 was not phosphorylated in Ubc13-deficient keratinocytes (Fig. 6*E*). Furthermore, luciferase assay confirmed the impaired activation of NF-κB pathway (Fig. 6*D*). Because Ubc13 is a polyubiquitin-conjugating enzyme, ubiquitination of IKK-γ was studied using immunoprecipitation. As shown in Fig. 6*F*, ubiquitination of IKK-γ by IL-1β was impaired in Ubc13-deficient keratinocytes. Thus, p38, JNK, and NF-κB pathways were impaired in Ubc13-deficient keratinocytes.

Heparin-binding EGF-like growth factor (HB-EGF) is a ligand for the EGF receptor and is a potent mitogen for keratinocytes (23). We tested whether HB-EGF-induced ERK activation was also impaired in *Ubc13*$^{flox/flox}$K5-Cre keratinocytes. We found that phosphorylation of ERK by HB-EGF was not impaired (Fig. 6*G*), indicating that overall cellular signaling was not impaired in *Ubc13*$^{flox/flox}$K5-Cre keratinocytes.

DISCUSSION

In the present study, we found that Ubc13 is essential for the growth, differentiation, and survival of mouse keratinocytes. Although Ubc13 regulates NF-κB signaling, the skin phenotype of the *Ubc13*$^{flox/flox}$ K5-Cre mice was different from that of TAK1- or IKK-γ-deficient epidermis. Epidermis-specific deletion of TAK1 or IKK-γ causes inflammation, abnormal keratinocyte differentiation, and keratinocyte apoptosis in the mouse skin (14, 24). The development of similar skin phenotypes among these mice indicates the disruption of a common cascade in the keratinocytes of these mice. Although an epidermal